NASA TM X-484

TECHNICAL MEMORANDUM

X-484

WEIGHTLESSNESS EXPERIMENTS WITH LIQUID HYDROGEN IN AEROBEE SOUNDING ROCKETS; UNIFORM RADIANT HEAT ADDITION - FLIGHT 1

By Richard H. Knoll, George R. Smolak, and Robert R. Nunamaker

Lewis Research Center
Cleveland, Ohio

NATIONAL AERONAUTICS AND SPACE ADMINISTRATION
WASHINGTON
June 1962

NATIONAL AERONAUTICS AND SPACE ADMINISTRATION

TECHNICAL MEMORANDUM X-484

WEIGHTLESSNESS EXPERIMENTS WITH LIQUID HYDROGEN IN AEROBEE SOUNDING ROCKETS; UNIFORM RADIANT HEAT ADDITION - FLIGHT 1*

By Richard H. Knoll, George R. Smolak,
and Robert R. Nunamaker

SUMMARY

A near-zero-gravity hydrogen heat-transfer experiment was conducted for a period of about 4 minutes in an Aerobee 150A sounding rocket. The primary objectives of this experiment were (1) to determine the fluid configuration under conditions of weightlessness and (2) to determine the heat transfer between a container wall and a fluid in a weightless environment.

The apparatus consisted of a thin-walled spherical hydrogen container surrounded by a radiant heater, which provided a source of heat flux representative of that which would be absorbed by an earth-orbiting bare stainless-steel tank. The outer surface of the hydrogen container was instrumented with temperature sensors, which provided a means of determining whether the wall was liquid wetted or vapor wetted.

For approximately one-half of the flight, liquid hydrogen completely wetted the walls. About 160 seconds after rocket sustainer burnout, a portion of the spherical container started to "dry." This vapor-covered area continued to increase during the remainder of the flight and eventually covered about one-half of the sphere area. A small sinusoidal g force and a failure to recover motion pictures during this flight prevented a positive conclusion regarding the equilibrium fluid configuration during weightless periods.

The measured wall temperatures indicated that the liquid adjacent to the wall was near the saturation temperature determined by the sphere pressure. This condition persisted even when large areas of the wall were vapor covered and at higher temperatures. The fact that the liquid-wetted wall temperatures and saturation temperatures were considerably higher than the calculated bulk temperature (based on the known heat impact and uniform mixing) indicated that some degree of stratification had taken place. Consequently, the calculated pressure rise was considerably lower than that measured during flight.

*Title, Unclassified.

INTRODUCTION

Liquid behavior in a weightless environment is a problem of importance to space vehicles employing liquids for propellants, coolants, or other purposes. Until the behavior of liquids in this environment is more predictable, it will be difficult to provide reliable answers to basic questions concerning venting of vapor instead of liquid from propellant tanks, collection of liquid propellants (especially those that are easily vaporized) after long coast periods, excessive pressure build-up in propellant tanks due to temperature stratification in the liquid, and nucleate and film boiling phenomena.

Basic to all of the preceding questions is a knowledge of the fluid configuration under conditions of weightlessness both with and without heat transfer. Many analytical and experimental attempts have been made to gain a better understanding of these phenomena. The behavior of liquids in a zero- or near-zero-gravity environment was studied analytically in references 1 to 3 and experimentally in references 4 and 5. With no heat transfer it has been generally concluded that the equilibrium configuration will depend upon the relative magnitude of the intermolecular forces (adhesion and cohesion). With heat transfer it is not known how the formation of vapor (as in boiling) will affect the equilibrium configuration. In a weightless environment buoyancy forces and free convection will no longer exist and hence leave no obvious means of removing the vapor from the wall. Reference 2 predicted that for a wetting fluid like hydrogen, the vapor bubbles formed on the wall would grow and eventually join the larger vapor bubble in the center of the tank. Reference 6 also predicted that hydrogen would remain on the wall with heat transfer. Others (refs. 7 and 8) believed that the transition from nucleate boiling to film boiling should occur at a very low rate of heat transfer and that the vapor would remain on the wall.

Several analytical and experimental attempts have been made to determine the effect of weightlessness on the heat-transfer mechanism. Some authors (e.g., ref. 9) proposed that in a normal gravity field the stirring action caused by the growth of bubbles is the primary factor in the heat-transfer mechanism. The reduction of gravity is thus implied to have little effect on the boiling mechanism. Recent boiling experiments with liquid nitrogen (ref. 10) and liquid hydrogen (ref. 11) indicated little or no change in the nucleate boiling curve (heat flux plotted against temperature difference) in a near-zero-gravity environment. For the liquid nitrogen data, however, the burnout flux did decrease with the lower gravitational field. The relative change in burnout flux was approximately the same as that obtained with water in reference 12, where the burnout flux decreased with reductions in gravity. Pool boiling experiments with Freon 114 using about 0.75 second of near weightlessness (ref. 13) indicated that the transition from nucleate to film boiling occurred at heat fluxes that permitted only nucleate boiling in a 1-g field. These data all indicate that film boiling will take place with lower heat fluxes in a zero-gravity field.

Thus far, most zero-gravity experiments have been limited to 1 or 2 seconds in drop towers and to approximately 10 to 20 seconds in airplanes. This experiment is the first in a series of zero-gravity experiments being conducted with Aerobee sounding rockets that are capable of providing approximately 5 minutes of zero gravity.

The purpose of this experiment was to determine the configuration of liquid hydrogen under conditions of weightlessness with heat transfer and to determine the effect of weightlessness on the heat-transfer mechanism. The scope of the paper includes discussions of (1) the heat-transfer experiment, (2) the Aerobee zero-gravity facility and the major payload instrumentation, (3) flight trajectory and near-zero-gravity environment, (4) the resulting fluid motion during flight, and (5) the heat transfer to the fluid and the resulting pressure rise.

APPARATUS AND PROCEDURE

Heat-Transfer Apparatus

Two techniques were employed to satisfy the objective of being able to predict whether or not the walls of a hydrogen container would be wetted with liquid during prolonged periods of weightlessness with heat flowing into the container. These techniques were (1) to photograph the contents of the hydrogen container through a window in the container wall and (2) to design the heat-transfer aspects of the experiment so that a simple measurement of temperature on the exterior wall of the hydrogen container would permit a positive indication of the presence of liquid on the interior of the wall. The second objective of the program was to determine qualitatively the method by which heat was transported from the wall of a hydrogen container to the weightless liquid hydrogen. This objective could be satisfied with (1) definitive motion pictures to show the type of boiling and fluid position and (2) instrumentation to indicate the thermal environment and heat-absorption rate at the external surface of the container. The shape of the hydrogen container was chosen as a sphere to provide geometrical symmetry, and specific efforts were made to eliminate, wherever feasible, objects within the container that might have some effect on the weightless configuration of the liquid hydrogen.

The spherical hydrogen tank, which had a low thermal diffusivity, was placed in a thermal environment where it was intended that the heat be transferred to the container almost entirely by radiation. The apparatus consisted of a 9-inch-diameter, 0.010-inch-thick stainless-steel hydrogen sphere contained in a larger 11-inch-diameter, 0.032-inch-thick stainless-steel sphere (fig. 1). The outer sphere contained cooling coils in which liquid nitrogen was passed to maintain a skin temperature near 140° R. A vacuum environment (about 0.01 micron) was maintained between the concentric spheres in order to reduce the heat transfer due to gaseous conduction. Suspended between the hydrogen sphere and the outer wall

was a concentric, 10-inch-inside-diameter, 0.016-inch-thick copper heater that provided the predetermined radiation environment for the experiment. The design value of heat-transfer rate to the hydrogen sphere was a nominal 160 Btu per hour per square foot, which corresponded to the rate of heat absorption by a typical bare cryogenic tank exposed to thermal radiation from the sun.

Mounted on the outer surface of the hydrogen sphere were 18 platinum resistance temperature transducers. The thin wall provided an effective means of determining whether liquid or vapor was adjacent to the wall. With liquid on the inner wall, the wall would be nearly at liquid temperature. When the wall was not liquid wetted the temperature at that position would rise abruptly because most of the incoming heat would go into the wall. The response of the transducers to step changes in heat-transfer rate through the wall was an important factor in permitting a deduction to be made concerning the presence or absence of liquid hydrogen on the hydrogen container inner surface at the location of each transducer (see appendix A).

On the inner surface of the sphere was mounted a liquid-level indicator, which consisted of a "ladder" with several evenly spaced rungs. The amount of hydrogen in the sphere was determined by direct observation of this precalibrated ladder prior to launch. The inner surface of the sphere had a 15-microinch surface finish.

In order for radiation to be the primary mode of heat transfer to the hydrogen container, several restrictions were applied to the design of solid conduction paths leading to the hydrogen sphere. Hydrogen filling and venting operations were accomplished through concentric stainless-steel tubes near the top of the container (see fig. 1). The tube outside diameters were 0.253 and 0.451 inch. Tube wall thicknesses were 0.003 and 0.007 inch, respectively. The hydrogen sphere was supported from the nitrogen cooled outer jacket by a Kel-F ring having numerous cutouts to decrease its heat conducting ability. The remaining solid conduction path was through the temperature transducer lead wires that ran from the base of the hydrogen sphere to a terminal plate bolted to the nitrogen cooled structural sphere. These 36 leads were each nylon clad insulated, 0.005-inch-diameter, 5-inch-long copper wire. Calculations estimating the magnitude of these heat leaks and other heat leaks are given in appendix A.

Two sapphire windows were provided in the hydrogen sphere (fig. 1). One window was used to provide optical access to the interior of the hydrogen sphere for the movie camera system. The other window furnished illumination for the movies with a stroboscopic light system. There was no solid heat conduction path between the sphere windows and any component other than the hydrogen sphere.

The heater was supported from the nitrogen cooled wall with 12 insulated clips. Each half (hemisphere) of the heater was spun from 0.016-inch copper sheet. The temperature of the heater was adjusted by varying the amount of electrical energy supplied to it. This electrical energy was dissipated in a resistance element coiled on and brazed to the external surface of each copper hemisphere. The resistance elements were actually Nichrome wire insulated with aluminum oxide. This insulated wire was inserted into a copper tube and the assembly was swaged. The ends were then hermetically sealed to prevent outgassing during the experiment. Transient testing of the temperature distribution over the surface of simulated hemispheres showed that the high thermal conductivity of the copper kept temperature gradients below a few degrees Fahrenheit. These small temperature gradients gave a uniform source of thermal radiation. Two platinum resistance temperature transducers were mounted on the external surface of each hemisphere.

High emissivity of the radiating surfaces (the inner surface of the heater hemisphere and the outer surface of the hydrogen sphere) was provided by painting them with flat black paint (military spec., MIL-E-10687A-Black) approximately 0.0005 inch thick. The emissivity and absorptivity of the painted surfaces were temperature dependent (appendix A). They varied from 0.47 at 180° R to 0.87 at 500° R and higher temperatures.

With this apparatus and the level of heat flux used, the heat leak due to solid conduction paths amounted to less than 1 percent. The heat leak due to gaseous conduction in the vacuum space was a function of vacuum (fig. 2). The normalized gaseous conduction plus radiation is plotted against indicated vacuum in microns. Gaseous hydrogen was bled into the vacuum space to vary the vacuum because it would give the largest heat-transfer rate. (Gaseous conduction is inversely proportional to the square root of the molecular weight; see appendix A.) Although there is considerable scatter in the data, it can be concluded that gaseous conduction will be negligible for vacuums less than 0.03 micron. Hence, with a vacuum of less than 0.03 micron, the heat-transfer rate to the hydrogen sphere can be predicted by thermal radiation equations alone from a knowledge of only the heater and sphere temperatures (appendix A).

Zero-Gravity Facility

The Aerobee 150A sounding rocket was used to simulate a zero-gravity environment. Since the Aerobee is spin stabilized, a spin-stabilized platform was necessary to maintain the payload at a zero-spin rate. The rocket contained helium thrust nozzles, which were used to compensate for the anticipated air drag encountered immediately after sustainer burnout and hence to extend the zero-gravity period. With the payload weight used (301 lb), a zero-gravity period of approximately 280 seconds was feasible.

The payload contained several measurements to help define the zero-gravity environment (fig. 3). There were two accelerometers in the longitudinal axis having full-scale readings of $\pm 10^{-2}$ and $\pm 10^{-3}$ g and two accelerometers in the lateral axis (90° out of phase with each other) with full-scale readings of $\pm 10^{-2}$ g. Magnetic aspect indicators were on board to give the relative position of the payload and to also detect whether the payload was spinning with respect to the local lines of magnetic flux.

The apparatus was instrumented to give heater temperatures, sphere temperatures, sphere pressure, and vacuum. This data and all other rocket performance parameters were telemetered to receiving stations at Wallops Island and Cape Canaveral.

Procedure

Several special prelaunch cryogenic handling procedures and flight procedures were employed.

The inner surfaces of the hydrogen sphere were cleaned by flushing the sphere with liquid trichloroethane and then purging it with dry helium gas. The surfaces forming the vacuum space were also cleaned with liquid trichloroethane. Outgassing of the heaters was minimized by cycling the temperature of the heaters between room temperature and 200° F several times while vacuum pumps were attached to the vacuum jacket. Vacuum pumping was continued with the apparatus at room temperature until just prior to the flowing of cryogenics to various parts of the sphere. At this time the vacuum jacket was sealed and the vacuum pump was disconnected.

Cryogenic flow was initiated by forcing liquid nitrogen flow through the cooling coils on the structural walls. This flow of nitrogen was maintained until the instant at which the apparatus was launched. When the cooling effect of the liquid nitrogen had greatly reduced the temperature of the internal components, liquid hydrogen flow was started. When equilibrium temperature conditions were established several hours later, the level of liquid hydrogen in the container was set and confirmed visually. At this time the hydrogen fill line was sealed. The hydrogen vent line was open to essentially atmospheric pressure at all times until launch.

At 2.3 hours before launch the final visual check of liquid hydrogen level in the container was made. At this time the liquid hydrogen was observed to be at the sixth rung from the top of the ladder used to detect liquid level. This level corresponded to a liquid volume of 30.3 percent of the hydrogen sphere volume.

At launch the hydrogen vent was automatically closed and the nitrogen supply line was automatically disconnected. The despin mechanism, all instruments, and telemetry were activated. Forty seconds after launch the camera and stroboscopic light were put into operation. At burnout the helium thrust nozzles were turned on to counteract the aerodynamic drag. At 95 seconds after launch, electric power was supplied to the copper radiant heaters. The recovery capsule containing the camera and film was separated at 350 seconds.

RESULTS AND DISCUSSION

Trajectory and Zero-Gravity Environment

An Aerobee rocket with a symmetrically heated 9-inch spherical Dewar containing about 22.5 percent by volume of liquid hydrogen was launched from Wallops Island, Virginia, on February 5, 1961. The results reported herein are based on telemetered data received at Wallops Island from the rocket. The recovery capsule, containing the movie camera and film, was separated after 350 seconds of flight and was parachuted into the Atlantic Ocean. Air and surface craft were unsuccessful in retrieving the capsule. The trajectory of the Aerobee is shown in figure 4(a). Sustainer burnout occurred at 53 seconds and an altitude of 19 nautical miles. The maximum altitude (apogee) of 81 miles was reached at approximately 215 seconds. Telemetered magnetic aspect indicator data indicate that the package remained relatively stable throughout most of the flight (figs. 4(b) and (c)). The package did not cone or rotate. At approximately 330 seconds a turnover occurred, probably because of aerodynamic drag.

The accelerations imposed upon the payload during flight are shown in figure 5. The ordinate ($n = a/g_o$) is in terms of a fraction of the normal gravitational acceleration. (See appendix B for a definition of all symbols.) Also plotted in these figures is the level ($n_* = \sigma_{st}/\rho g_o L^2$) at which the forces resulting from the inertial accelerations are approximately equivalent to those due to capillary phenomena (ref. 1). Figure 5(a) shows the longitudinal accelerations imposed upon the sphere during flight. Prior to sustainer burnout the payload was subjected to relatively high accelerations (of the order of 10 g). Just after burnout a negative acceleration was experienced (-6×10^{-3} g) because the aerodynamic drag forces exceeded the thrust from the helium thrust nozzles. From 56 to 88 seconds the acceleration was positive, because the helium thrust exceeded the aerodynamic drag. From

88 seconds (after the helium thrust nozzles ceased to operate) to 330 seconds, the accelerations in the longitudinal axis were $\leq \pm 10^{-4}$ g. Reference 1 indicates that in order for the capillary phenomenon to become significant n_* should be $<<4.7\times10^{-4}$ g. In the longitudinal axis, this requirement was met from 88 to 330 seconds.

Figure 5(b) shows the lateral acceleration history during the flight. Both lateral accelerometer outputs varied sinusoidally with an amplitude of $\pm 2\times10^{-2}$ g and a frequency of 2.5 cps. The estimate of the amplitude was based on an extrapolation of the sine curve. Also plotted on this figure is the information from the solar aspect indicators that were located on the spinning Aerobee. The frequency of the accelerometer output was the same as that of the spinning Aerobee. It is thus concluded that the sinusoidal output of the lateral accelerometers was the result of a slight misalinement between the rocket and the spin stabilized platform axes. The accelerations given are those experienced 3 inches from the centerline of the rocket. (The outermost wall of the sphere would experience accelerations 1.5 times as high as those shown in fig. 5(b)). These accelerations are about two orders of magnitude higher than n_*, but because of the oscillatory motion this type of acceleration might not have the same effect as a constant acceleration.

Fluid Motion and Fluid Configuration

The motion of the fluid during the flight can best be described with the sphere temperatures (fig. 6). In figure 6(a) the temperatures in degrees Rankine of transducers 15, 17, 12, 10, and 6 are shown against time after launch in seconds. The location of these temperature transducers on the sphere is shown in the accompanying sketch (and also in appendix A). Figure 6(b) gives the remaining transducers (2, 3, 4, 5, and 8). The temperatures shown have been adjusted as discussed in appendix A. Also plotted in these figures is the saturation temperature of the hydrogen corresponding to the flight sphere pressure. Figure 7 shows the heater temperatures in degrees Rankine plotted against flight time. Several significant events are also noted to help interpret the fluid motion (i.e., rocket sustainer burnout, time when heaters are turned on, and separation).

In figure 6 the temperatures indicate that the hydrogen remained in the bottom of the container during boost with a temperature profile increasing from the bottom to the top of the hydrogen sphere. The sphere contained about 22.5 percent liquid by volume at lift-off.

Soon after burnout (53 sec), the entire sphere became liquid wetted. This is evident by the sharp decrease in temperatures on figure 6(a). According to reference 1, the time required to modify the 1-g configuration to that which would persist in zero gravity is approximately 4.6

seconds for this experiment. The rapid wetting off the walls was probably caused by a combination of the following factors: (1) negative longitudinal acceleration (fig. 5(a)), (2) fluid inertia, (3) system vibrations at sustainer thrust termination, and (4) oscillatory radial acceleration.

From 56 to 88 seconds the container was subjected to a positive g (fig. 5(a)) and from the temperature histories it appears that the walls remained liquid wetted. The accelerations experienced at this time (about 10^{-2} g) were much larger than n_* and the liquid might be expected to be pulled away from the upper half of the sphere. However, motion pictures taken during subsequent experiments indicate fluid circulation during this period and hence would invalidate the n_* criterion.

From 88 to 216 seconds all temperature transducers with the exception of number 15 (see sketch on fig. 6(a)) indicated temperatures near the liquid temperature. At 110 seconds number 15 began to increase in temperature. This increase indicates that vapor next to the wall caused a decrease in the rate of heat transfer away from the wall and hence an increase in the amount of heat absorbed by the wall. Then, at approximately 140 seconds, the wall was covered with liquid again. The reason for this temporary drying of the wall in the vicinity of transducer 15 is not known but it indicates some movement of the fluid. The remaining wall temperatures during the period 88 to 215 seconds tended to follow the saturation temperature determined from the sphere pressure. Although there is a $\pm 2^{\circ}$ R accuracy in the temperatures, it is apparent that there is a definite relation between the saturation temperature and the wall temperature.

At 215 seconds the tank wall in the vicinity of temperature transducer 15 became covered with vapor, as indicated by the rapidly rising temperature in figure 6(a). Shortly thereafter, transducers 17, 10, 6, and 12 indicated vapor on the wall. It is not known why the drying of the wall occurred. Several possibilities are listed:

(1) The top of the sphere may have been covered by a thin layer of liquid that completely vaporized.

(2) Vapor may have been emitted from the fill or vent line and may have created a locally dry wall which continued to grow in size.

(3) The fill neck provided a localized hot spot which may have initiated the vapor film.

(4) The formation of a vapor layer may have been a result of the bubbles not leaving the wall.

Despite the cause of the vapor formation, once an area of the wall dried, the drying process continued.

At approximately 330 seconds the vehicle began to turn over as indicated by the magnetic aspect data (fig. 4) and the accelerometer data (fig. 5). Sphere temperatures shown in figure 6 also verify this conclusion. The bottom temperatures started to increase sharply at about 330 seconds (transducers 2, 3, 4, and 5) and the upper temperatures (transducers 15, 14, 12, and 10) decreased rapidly shortly thereafter. The force imposed upon the sphere during the course of the turnover was less than 10^{-3} g. The physical rotation of the sphere around the liquid, however, appears to have caused the translation of the fluid with respect to the wall rather than the 10^{-3} g force to have caused the liquid to leave the bottom and strike the top.

Heat Transfer

Effect of reduced gravitational field on heat transfer. - The heat absorbed by the hydrogen was determined from heater temperatures, sphere temperatures, emissivities of the surfaces, solid conduction heat leaks, vacuum, and so forth as discussed in appendix A. With the heater temperatures (fig. 7) and the sphere temperatures (fig. 6(a)), the radiant heat-transfer rate to the hydrogen container was calculated. The rate of gaseous conduction to the hydrogen container was based on a vacuum of 0.04 micron, which was the best estimate available in lieu of actual flight measurement.

The results of the heat-transfer calculations are given in figure 8 where the average rate of heat absorption by the hydrogen mixture in Btu per hour per square foot is plotted against time. An average heat-absorption rate was calculated for each heater hemisphere. The arithmetic average of these two values is plotted in figure 8. The heat-absorption rate changes rapidly from 100 to 200 seconds because of the increasing heater temperatures. For the remainder of the experiment the heat-absorption rate levels off at about 270 Btu per hour per square foot. (The solar flux at the earth's distance from the sun is 430 Btu/(hr)(sq ft).) A slight decrease in heat-absorption rate occurs at 215 and 280 seconds. This decrease is a result of the increase in wall temperature (caused by vapor adjacent to the wall) and hence the absorption of a portion of the incoming heat flux by the wall. Shortly after 325 seconds the rate of heat absorption by the hydrogen mixture correspondingly increased because of the heat absorbed when the liquid passed over the relatively warm wall during the turnover.

The preceding calculations of hydrogen heat absorption rates were made without the necessity of understanding the mechanism(s) by

which this heat was transferred from the wall of the Dewar to the hydrogen. At this point it is pertinent to examine the possible modes of heat transfer to account for these calculated heat-absorption rates. Since, in a zero-gravity field, free convection currents and buoyancy forces are no longer present, heat transfer should take place by (1) thermal conduction through the liquid, (2) thermal conduction through the vapor, (3) radiation, (4) a process similar to boiling, or (5) a combination of these methods. For this experiment the 10^{-2} g sinusoidal acceleration could have increased the heat transfer slightly in a boiling process by helping remove vapor or could have caused some form of forced convection. There would be no effect on conduction or radiation.

Heat transfer through the liquid by conduction alone can be eliminated by a simple calculation of the temperature drop required to support the imposed heat flux as shown in figure 9. The temperature gradients required for conduction through various thicknesses of vapor are also shown. The horizontal line is the experimental heat flux level. The temperature gradients necessary for conduction of even relatively low heat fluxes through the liquid soon require a wall temperature in excess of the critical temperature (the highest temperature at which the liquid can exist). Conduction through a vapor layer, however, is possible for very small thicknesses of vapor (< 0.001 in.) and relatively small temperature drops.

Heat transfer by thermal radiation from the inner wall is small because of the low wall temperatures. For example, the maximum amount of heat due to radiation from a 200° R wall that could be absorbed by the hydrogen is 2.74 Btu per hour per square foot, which is much lower than the 270 Btu per hour per square foot level.

Heat transfer by a process similar to boiling could provide the relatively high heat fluxes. The heat-flux level experienced during this experiment very closely approached the lower level of 1-g nucleate boiling curves given in references 14 to 16. These data are plotted on figure 10. The temperature differences ΔT given are between the heating surface and the bulk of the liquid. The horizontal line represents the approximate heat-transfer rate used in the experiment (270 Btu/(hr)(sq ft)). Apparently nucleate boiling does exist for the heat-flux levels used.

Curves 1 and 4 on figure 10 show the effect of increasing pressure on the ΔT required for nucleate boiling. For the heat flux used in this experiment, it appears that the ΔT is of the order of 1° R or less since the pressure in the experiment ranged from 1 to 10 atmospheres. From the recorded wall temperatures it was not possible to determine a 1° R temperature difference because of the $\pm 2^{\circ}$ R accuracy; however, an estimate of ΔT can be made as indicated in figure 11. The saturation temperature is compared with the calculated bulk temperature, which is

the temperature the fluid would assume if all the heat absorbed were distributed uniformly throughout the hydrogen mixture. (The uniform mixture calculation gave excellent agreement with the results of experimental ground tests as shown in appendix A.) The calculated bulk temperature represents an upper limit of the actual bulk temperature of the liquid. The saturation temperature represents the lower limit of the wall temperature because the inner wall has to be at least as high as the saturation temperature in order for bubbles to form. From figure 11, the temperature difference between the two curves increases with time and is of the order of 0° R at 200 seconds and 3° R at 330 seconds. Although this is an estimate of ΔT, it is apparent that it is of the same order of magnitude as the 1-g boiling data given in figure 10. Recent experiments with liquid nitrogen (ref. 10) and liquid hydrogen (ref. 11) indicate little or no shift in the nucleate boiling curve with reductions in gravity.

The presence of the small sinusoidal force due to misalinement of the spin-stabilized platform raises the question as to whether forced convection could have supported the relatively high heat fluxes. An estimate of the velocity of the fluid relative to the inner wall required to transport 270 Btu per hour per square foot yielded about 5.7 feet per second (appendix A). Motion pictures from recent flights indicate that there was very little motion due to the sinusoidal forces ($\ll$5.7 ft/sec). Hence, convection alone could not have accounted for the high heat fluxes. The drying off of the upper portion of the hydrogen sphere (fig. 6(a)) also indicated that the relative motion of the liquid was not sufficient to keep the walls wet. (If drying had occurred because of this force, it would first occur at the axis of rotation and hence give two dry areas diametrically opposite each other.)

From these considerations it can be concluded that vapor must be formed on the inner tank wall (with the heat flux used) either in the form of a thin layer or in the form of bubbles as in nucleate boiling. For static-pressure equilibrium the temperature of any liquid-vapor interface in the system would have to be that of the saturation temperature. Thus the layer of liquid adjacent to the wall would be bounded by temperatures at least as high as the saturation temperature. The calculated bulk temperature is lower than the saturation temperature. The exact cause of this temperature gradient is not known. Three possible explanations are (1) the movement of a bubble from the wall to the interface could transport heat, (2) the formation of a bubble displaces a given volume and hence compresses the remaining fluid and causes condensation to take place at the liquid-vapor interface, and (3) the violent boiling at the periphery of the drying area might eject warm liquid droplets (as water on a hot skillet) that would strike the interface and warm it, or vapor formed in this area could recondense on the cooler interface and hence warm it.

Another result apparent from figure 6(a) is that despite the relatively high wall temperatures of the vapor covered wall, the wall area that was covered with liquid was at a temperature close to that of the saturation temperature.

Effect of reduced gravitational field on pressure rise. - An important consideration for the design of cryogenic systems for space flight is an adequate knowledge of the thermodynamic state of the fluid. This can be best demonstrated for this experiment by referring to figures 12 and 13. In figure 12 the actual pressure during flight is compared with the pressure that would be obtained if all the heat went into raising the bulk temperature of the fluid (i.e., uniform fluid temperature throughout). The pressures do not increase significantly until the heater reaches near full temperature at 180 seconds. The homogeneous (uniform temperature) pressure rise was calculated from the heat input and a knowledge of the amount of liquid in the sphere (see appendix A). It is apparent from figure 12 that the homogeneous pressure is somewhat lower than that measured during flight.

In figure 13 the measured pressure and homogeneous pressure for three different fillings are shown against the total amount of heat absorbed. This figure presents a more representative picture of the pressure difference since the pressure depends upon the amount of heat absorbed for the homogeneous case and hence would be expected to be a primary factor in the actual pressure rise. From the figure it is apparent that the measured pressure deviates considerably from the calculated pressure for the 22.5 percent filling. Up to 100 pounds per square inch absolute it appears as if the 14.2 percent filling closely approximates the pressure rise. Beyond 100 pounds per square inch absolute the pressure continuously deviates from this filling and crosses the 7.3 percent filling line at 140 pounds per square inch absolute. The deviation of the measured pressure from the calculated pressure for the 22.5 percent filling indicates that the heat was not distributed uniformly throughout the mixture and that a phenomenon similar to stratification took place.

Several investigations (refs. 17 and 18) have been made of this so-called stratification phenomenon of cryogenic fluids in closed containers in a normal gravity field. They observed that for a given heat input the corresponding pressure level is always higher than that of a uniformly mixed fluid. This higher pressure results because a thin, warm layer of liquid builds up at the liquid-vapor interface (ref. 19) because of density gradients, low thermal conductivity of liquid hydrogen, and the method of heat input. The bulk of the fluid is usually at some lower temperature but the pressure in the system is determined by the temperature of the interface. Once a stratified liquid is disturbed and the liquid is mixed a pressure drop results. Although gravity helps to support stratification (ref. 19), this nonequilibrium condition may also exist in a near-zero- or zero-gravity environment.

A convenient representation of the effect of stratification is shown in figure 14. The difference between the actual pressure and the calculated homogeneous pressure is plotted against the total heat input per unit area. The pressure difference increases with increasing heat input. This nonequilibrium mixture could be of concern to tank designers. For example, if a hydrogen tank were continuously vented to maintain a given pressure and small rockets were fired to collect the liquid for restart (and hence to mix the fluid), the resulting pressure or net positive suction head might be lower than that anticipated. Although there is a definite deviation of the measured pressure from the calculated pressure for this experiment, it is not presently known how to scale the results to larger sized tanks.

CONCLUDING REMARKS

A near-zero-gravity liquid-hydrogen heat-transfer experiment was conducted for a period of about 4 minutes in an Aerobee 150A rocket. The primary objectives of the experiment were (1) to determine the fluid configuration under conditions of weightlessness with heat transfer into the hydrogen and (2) to determine the heat-transfer mechanism between a container wall and fluid in a weightless environment.

A heat flux of 270 Btu per hour per square foot was imposed upon a 9-inch-diameter sphere 22.5 percent full of liquid hydrogen. A 10^{-2} g sinusoidal acceleration due to spin-table misalinement was imposed upon the sphere throughout the flight. The liquid hydrogen completely wetted the container wall for approximately one-half of the flight. Near the apogee (at 215 sec) the upper portion of the container started to show vapor on the walls. This vapor pocket continued to grow during the remainder of the flight, eventually covering about one-half of the sphere area. Although it is not known how the vapor formation started, once the wall became partially dry it continued to dry with the heat flux used (270 Btu/(hr)(sq ft)).

Whenever the walls were wetted with liquid the wall temperatures were near the saturation temperature determined by the sphere pressure. This condition persisted even when an area of the wall was vapor wetted (partially dry) and at temperatures near 200° R.

Despite the ±2° R accuracy in the wall temperature measurement, it can be said that there is a definite relation between the measured wall temperatures and the saturation temperature determined from the sphere pressure. The two temperatures appear to be approximately the same within the indicated accuracy. An estimate of the bulk temperature of the fluid was made by assuming that all the heat absorbed was uniformly distributed throughout the hydrogen mixture. This estimate differed from

the saturation temperature by about 0° to 3° R, which is roughly the same order of temperature difference required for nucleate boiling of hydrogen in a normal gravity field, for the heat flux used. Inspection of the heat-transfer mechanisms indicated that a process similar to nucleate boiling would be required to transfer the given amount of heat.

The fact that the sphere pressure during the near-zero-gravity period was considerably higher than the calculated homogeneous pressure indicated that some degree of stratification took place. The difference between the measured pressure and homogeneous pressure increased with increasing total heat absorption by the hydrogen mixture. Light-weight tankage designed on the basis of uniform mixing could be inadequate in zero-gravity conditions because of this difference. Also, venting and pressurization requirements could be seriously affected.

Although a 10^{-2} g sinusoidal lateral acceleration was imposed upon the container throughout the flight the following still occurred: (1) the walls continued to "dry off" once a vapor wetted area was initiated and (2) the pressure continued to increase over the calculated homogeneous pressure. It is not known exactly what effect the slight g forces had on the configuration and heat transfer, but from the results of subsequent tests it is apparent that this oscillatory motion played a small role on the broad results.

Lewis Research Center
National Aeronautics and Space Administration
Cleveland, Ohio, February 28, 1962

APPENDIX A

HEAT-TRANSFER ANALYSIS AND INSTRUMENTATION

Temperature Instrumentation

The temperature transducers used on the hydrogen sphere and the heater consisted of small platinum resistance elements that gave resistances of approximately 2000 ohms at 37° R and 5000 ohms at room temperature. The platinum resistance element was painted on a wafer of aluminum oxide approximately 0.25 inch square by 0.006 inch thick. The aluminum oxide surface was cemented to the 0.010-inch sphere wall and then covered by a 0.5- by 0.5-inch stainless-steel radiation shield 0.003 inch thick. Mica was used to insulate the element from all metal contacts.

The response of a typical element mounted on the 0.010-inch wall compared with that of a thermocouple is shown in figure 15. Here it is assumed that the thermocouple gives the actual wall temperature. These results were determined by plunging the thermocouple and platinum resistance element (both mounted on a piece of 0.010-in. AM350 wall) into boiling liquid hydrogen. The slow response for the first 0.5 second is due to the nature of the testing conditions and should be disregarded. It is apparent that the platinum element (from 0.5 sec on) lags the thermocouple response by about 0.5 second. Good agreement is also obtained when the 0.010-inch wall is extracted from boiling liquid hydrogen and exposed to a relatively higher heat flux as shown in figure 16. The poor thermal conductivity of the vapor decreases the heat transfer away from the wall, causes the wall to absorb more heat, and hence increases the wall temperature.

The locations of the temperature transducers on the hydrogen sphere are as indicated in figure 17. In figure 17(a), the transducers for the lower half of the sphere are shown and in 17(b), those for the upper half. The Kel-F ring on the sphere equator is visible in both figures. (The number indicated for each platinum resistance element is used throughout the report.) Transducer number 1 (fig. 17(a)) is 1 inch from the tube used to thread through all the lead wires. Numbers 2, 3, 4, and 5 are 3.5 inches from the sphere equator (measured along the curved surface) and are positioned 90° apart. Numbers 6, 7, 8, and 9 are 1 inch from the sphere equator (also measured along the curved surface) and are 90° apart. The relative locations of all the transducers are indicated in figure 17(c). The transducers for the upper half follow the same pattern as for the lower half. Number 18 is also 1 inch from the fill and vent neck. The pattern used was an attempt to distribute evenly all the temperature measurements. Of the 18 transducers, flight measurements were obtained from 2, 3, 4, 6, 8, 10, 12, 15, and 17.

Heat-Transfer Equations

The amount of heat absorbed by the contained hydrogen is equal to the heat transferred to the sphere by radiation, solid conduction, and gaseous conduction less the amount of heat stored in the container itself. This heat is given by

$$\Delta Q_{abs} = (\dot{Q}_r + \dot{Q}_{sc} + \dot{Q}_{gc})\Delta t - \Delta Q_s \tag{A1}$$

The heat transferred by thermal radiation between two concentric spheres is a function of the boundary temperatures, emissivities, and diameters and is given by reference 19 as

$$\frac{\dot{Q}_r}{A_s} = \frac{\sigma\left(T_h^4 - T_s^4\right)}{\frac{1}{\epsilon_s} + \frac{A_s}{A_h}\left(\frac{1}{\epsilon_h} - 1\right)} \tag{A2}$$

This equation assumes that both surfaces are gray, which introduces little error in the calculations. It also assumes that the reflections are diffuse rather than specular and that both surfaces have uniform temperatures. Diffuse reflections are highly probable because of the painted flat black surfaces used. In calculating the radiant heat transfer, the temperature of each heater hemisphere was considered individually. For the high heater temperatures used, the calculation was insensitive to T_s because of the fourth-power difference.

The heat transferred by solid conduction is given by

$$\frac{\dot{Q}_{sc}}{A_{sc}} = \frac{k}{l}\Delta T \tag{A3}$$

The heat transferred by gaseous conduction is given by reference 19 as

$$\frac{\dot{Q}_{gc}}{A_s} = K\left(\frac{\gamma + 1}{\gamma - 1}\right)\left[\frac{\alpha_s\alpha_h}{\alpha_h + \alpha_s(1 - \alpha_h)\frac{A_s}{A_h}}\right]\left(\frac{P_G}{\sqrt{MT_G}}\right)(T_h - T_s) \tag{A4}$$

where K is a numerical constant that depends on the units used.

The heat absorbed by the container wall is a function of the specific heat, the weight of the container, and the temperature change and is given by

$$\Delta Q_s = WC_p \Delta T_s \qquad (A5)$$

In order to simplify the heat-transfer calculations, the solid support conduction and gaseous conduction were designed to be negligible in comparison with the heat transferred by radiation. With these two sources of heat transfer at a minimum, relative to the radiant heat transfer, the total heat transferred to the hydrogen can be reasonably determined with only the heater temperatures and sphere temperatures.

Surface Emissivity and Radiant Heat Transfer

The emissivity of the two surfaces involved in the radiation exchange was temperature dependent (fig. 18).

The absorptivity of the hydrogen sphere was the same as the emissivity of the warmer heater. When equal values for the absorptivity and the emissivity were used to calculate the pressure rise in a ground test, the calculated pressure was in good agreement with the pressure measured (see section Pressure Rise Calculations). The heat-transfer rate due to radiation from the heater during flight is shown in figure 19. Also shown are the contributions of the heat leaks.

Calculation of Heat Leaks

Solid conduction. - The solid conduction paths to the hydrogen sphere consisted of the temperature instrumentation leads, the fill and the vent tubes, and the Kel-F support ring on the sphere equator (see fig. 1).

The instrumentation leads consisted of 0.005-inch-diameter nylon insulated copper wire. Each lead wire (a total of 36 wires for 18 temperature elements) was bonded to the sphere surface, led down to the bottom of the sphere, and terminated at a Fusite fitting in the nitrogen cooling jacket. Approximately 5.5 inches of lead wire connected the hydrogen sphere and the nitrogen cooling jacket. Skin temperature measurements during simulated preflight conditions indicated that the temperature of the Fusite fitting T_F was 170° R. Therefore, the heat conducted through the wires is given by equation (A3) as

$$\dot{Q}_L = \frac{A_L N}{l} k_{Cu} (T_F - T_s) = 8.93 \times 10^{-7} k_{Cu} (170 - T_s), \text{ Btu/hr}$$

where k_{Cu} ((Btu)(in.)/(hr)(sq ft)(^{o}R)) is a function of $T_{avg} = (170 + T_s)/2$. By use of values of thermal conductivity from reference 17 and a sphere temperature T_s equivalent to an average given by temperature transducers numbers 2, 3, 4, and 5 (see fig. 6(b)), the heat leak was calculated for the flight. This heat leak and others are given in figure 19.

The conduction paths for the fill and the vent tubes consisted of a 4-inch-long, 0.253-inch-outside-diameter tube with a 0.003-inch wall and a 1.1-inch-long, 0.451-inch-outside-diameter tube with a 0.007-inch wall. The boundary temperatures for the fill tube are assumed to be 500^{o} R (from the skin-temperature measurement) and a temperature corresponding to the average of temperature transducers 15 and 17. For the vent tube, 170^{o} R was used for one boundary and an average of 15 and 17 for the other. Using equation (A3), the heat leak through the fill-vent tube is given by

$$\dot{Q}_{f-v} = 4.09\times10^{-6}\, k_{ss}\left(500 - \frac{T_{15} + T_{17}}{2}\right) + 6.16\times10^{-5}\, k_{ss}\left(170 - \frac{T_{15} + T_{17}}{2}\right), \text{ Btu/hr}$$

where k_{ss} is the thermal conductivity of stainless steel ((Btu)(in.)/(hr)(sq ft)(^{o}R)) (ref. 19) at an average temperature of

$$T_{avg} = \frac{500}{2} + \frac{T_{15} + T_{17}}{4}$$

for the fill tube and

$$T_{avg} = 85 + \frac{T_{15} + T_{17}}{4}$$

for the vent tube.

The conduction through the equator support ring is difficult to determine because of the shape of the conduction path as shown in the sketch. Hence, conservative assumptions were made in order to maximize

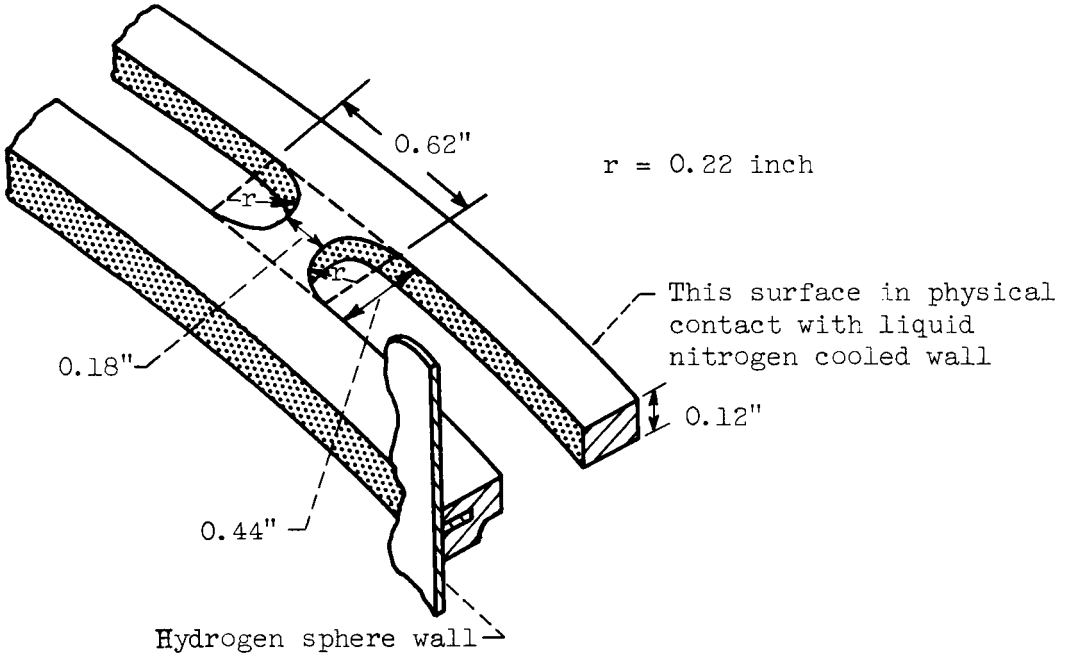

the heat leak. There are a total of eight support members of the type shown. An effective width of the conduction path is obtained by dividing the area of the rectangle, indicated by the dashed line, less the area of a 0.22-inch-radius circle by the length of 0.44 inch, which yields 0.275 inch. The thickness of the Kel-F through the supporting member is 0.12 inch. The boundary temperatures are assumed to be 190° R and the temperature of the sphere in the area of the equator, which is obtained by averaging the temperatures from transducers 6, 10, and 12. By use of equation (A3), the heat conducted through the support ring is

$$Q_{sr} = 2.085 \times 10^{-3} \, k_{sr} \left(190 - \frac{T_6 + T_{10} + T_{12}}{3} \right), \text{ Btu/hr}$$

where k_{sr} is assumed to be 1.53 (Btu)(in.)/(hr)(sq ft)(°R) for all temperatures between 190° and 37° R.

Radiation. - The heat leaks due to radiation arise from the cutouts in the heater for the camera port, the light source port, the fill and the vent tubes, the support ring, and the tube through which all the temperature instrumentation wires are threaded. Actually, the cutouts are

areas where the heat flux is much less than the design flux, but they must be considered because the radiant heat transfer to the hydrogen sphere is defined as

$$\frac{\dot{Q}}{A_s} = \frac{\sigma\left(T_h^4 - T_s^4\right)}{\frac{1}{\epsilon_h} + \frac{A_s}{A_h}\left(\frac{1}{\epsilon_s} - 1\right)} \left(1 - \frac{A_{cutout}}{A_h}\right) \tag{A6}$$

An approximation of the heat leak due to radiation from the camera port can be obtained with the following equation for flat plates (ref. 19):

$$\dot{Q}_{r,c} = \frac{\sigma A(T_c^4 - T_s^4)\epsilon}{(2 - \epsilon)} = \frac{\sigma A \epsilon}{2 - \epsilon} T_c^4 - \frac{\sigma A \epsilon}{2 - \epsilon} T_s^4 \tag{A7}$$

For simplicity the emissivity of both surfaces involved are assumed to be equal; this assumption gives a conservative estimate of heat leaks. The radiating temperature T_c and emissivity are 540° R and 0.9, respectively. Using the above equation and the proper area, the heat-leak rate can be expressed as

$$\dot{Q}_{r,c} = 2.887 - 3.4\times10^{-11}\left(\frac{T_{15}^4 + T_{17}^4}{2}\right), \text{ Btu/hr}$$

The heat-leak rate due to the light source (see fig. 19) was found to be negligible. This rate was obtained by recording the change in boiloff rate caused by turning on the light under conditions simulating flight.

The heat-leak rates due to the other cutouts were approximated with the following equation:

$$\frac{\dot{Q}}{A_{cutout}} = \frac{\sigma(T_w^4 - T_s^4)\epsilon_w}{2 - \epsilon_w} + \sigma\epsilon_{Cu}(1 - \epsilon_w)\epsilon_h T_h^4, \tag{A8}$$

The first term is a simplification of the flat-plate equation (all emissivities equal) and represents the heat-transfer rate to the hydrogen sphere caused by radiation from the outer wall (nitrogen cooling shell). The second term is an approximation of the radiation that originates from the outer heater surface and is reflected off the outer wall toward the exposed hydrogen tank (in the area of the cutout). The emissivity of the relatively shiny cooling jacket wall ϵ_w was assumed to be 0.37. The emissivity of the outer surface of the copper heater, which was polished, was assumed to be 0.05, the value lying between that of mechanically polished copper and scraped copper (ref. 19).

By use of the preceding assumptions and the proper temperatures, the heat-leak rates due to the various cutouts are given by the following equations:

Fill-vent tube cutout:

$$\dot{Q}_{r,f\text{-}v} = 0.848\times10^{-11}\left(8.352\times10^{8} - \frac{T_{15}^4 + T_{17}^4}{2}\right) + 1.177\times10^{-12}\,\epsilon_h T_h^4, \text{ Btu/hr}$$

Equator cutout:

$$\dot{Q}_{r,sr} = 2.179\times10^{-11}\left(13.03\times10^{8} - \frac{T_6^4 + T_{10}^4 + T_{12}^4}{3}\right) + 3.022\times10^{-12}\,\epsilon_h T_h^4, \text{ Btu/hr}$$

Instrumentation lead tube cutout:

$$\dot{Q}_{r,ilt} = 1.225\times10^{-12}\left(8.352\times10^{8} - \frac{T_2^4 + T_3^4 + T_4^4 + T_5^4}{4}\right) + 1.7\times10^{-12}\epsilon_h T_h^4, \text{ Btu/hr}$$

Gaseous conduction. - The heat-transfer rate due to gaseous conduction is given by equation (A4) as

$$\dot{Q}_{gc} = 0.5733\,A_s\,\frac{\alpha_s\alpha_h}{\alpha_h + \alpha_s(1-\alpha_h)\frac{A_s}{A_h}}\left(\frac{\gamma+1}{\gamma-1}\right)\frac{P_G}{\sqrt{MT_G}}\,(T_h - T_s), \text{ Btu/hr}$$

The accommodation coefficient is a function of the residual gas and the surface temperature. For this calculation, it is assumed that the residual gas is hydrogen and that the variation of the accomodation coefficient with surface temperature is that given by reference 19. The temperature of the gas at the vacuum gage T_G is assumed to be 540° R. Even if T_G were 140° R (about the lowest temperature possible in this experiment), the gaseous conduction would be only about twice as large as that shown in figure 18. The specific-heat ratio also varies with temperature and is taken into account.

The contributions of all the heat leaks discussed are shown in figure 19. The radiant heat transferred from the heater to the sphere is also shown. It is apparent that the sum of all the heat leaks is at least two orders of magnitude less than the radiant heat transfer. The heat-transfer rate into the contained hydrogen mass is given by the

dashed line. This rate takes into account all heat leaks and the heat stored in the container wall.

Hydrogen Mass During Flight

The amount of liquid hydrogen in the sphere was determined by observing where the liquid level was with respect to a precalibrated ladder (see fig. 1). The last visual observation of the liquid level was made 2 hours and 18 minutes before launch. At that time, the sphere contained 30.3 percent liquid by volume (p = 30.3). In order to determine the amount of liquid left at launch, the liquid lost because of boiloff during this period must be known. Heat-leak data for the flight model experiment are not available; however, data from a similar experimental model are available and have been corrected to account for the differences in the models. These heat-leak data are plotted as a function of heater temperature in figure 20. The heater temperature at the time of the last visual observation of the liquid level was 254° R. From figure 7, the temperature at launch was 185° R and the average temperature was thus 220° R. The average heat-leak rate is therefore 6.4 Btu per hour.

The amount of liquid boiled off in percentage of total volume during the holding period is given by

$$p_{bo} = \frac{(\text{Boiloff rate}) \times (\text{time})}{h_v V \rho_{sl}} \times 100 \text{ percent}$$

where h_v is the heat of vaporization, V, the sphere volume, and ρ_{sl}, the density of saturated liquid. Hence

$$p_{bo} = \frac{(6.4)(2.3)(100)\text{percent}}{194(0.2208)(4.418)} = 7.8 \text{ percent}$$

This calculation leaves 22.5 percent at launch. The total mass in the container is given by

$$\text{Weight of } H_2 = \frac{pV\rho_{sl} + (100 - p)V\rho_{sv}}{100} = 0.2338 \text{ lb}$$

The specific volume of the system is given by

$$v = \frac{V}{\text{Weight of } H_2} = 0.9443 \frac{\text{cu ft}}{\text{lb}}$$

[redacted]

Pressure Rise Calculations

The heat input to the contained mass of hydrogen liquid and vapor can be obtained from the heat-transfer equations discussed previously. With this heat input and a knowledge of the mass of hydrogen, the pressure can be calculated for the constant volume system, which assumes that the contents are in thermal equilibrium. The equation for this process can be obtained from the first law of thermodynamics and the definition of enthalpy and is given as

$$q = \Delta H - v \Delta P \qquad \text{(A9)}$$

This equation checked experimental results quite accurately in the work described in reference 17.

In calculation of the pressure rise, the thermodynamic properties of para-hydrogen were needed. For this particular experiment, the properties of para-hydrogen were obtained from reference 20. The properties used are presented in figures 21 and 22. Figure 21 gives the saturation temperature against pressure; the temperature is given against the density of liquid hydrogen in figure 22(a) and the vapor density in figure 22(b). The plot of enthalpy against pressure for the constant volume process used in this experiment was obtained from reference 20 and is given in figure 23. A constant specific volume of 0.9443 cubic feet per pound was used as determined previously. With the enthalpy as a function of pressure, equation (A9) can be solved to give pressure against heat added as shown in figure 24 for the 9-inch-diameter sphere. The pressure is in pounds per square inch absolute and the heat added q is in Btu. For a determination of the pressure for a given heat addition, the initial pressure is needed to locate a starting point on the curve. The resulting pressure is then obtained by adding Δq to the initial q.

Several ground tests were performed to determine whether the pressure-rise equation and the heat-transfer equations were sufficiently accurate for the purposes of the experiment. The results of three of these tests are presented in figure 25. The conditions in these tests closely approximated those during flight with the exception that the container was shaken to maintain a uniform temperature fluid throughout. A known amount of liquid hydrogen was put into the sphere. The vent was then closed, the heaters were turned on and the contents were shaken. The pressure, heater temperatures, and sphere temperatures were recorded throughout the test. The calculated pressure was obtained using the heat-transfer equations and pressure equation presented in this appendix. It is apparent from figure 25 that the calculated pressure closely approximates the actual recorded pressure. These curves are significant in that they substantiate the entire range of assumptions and the calculation procedures used throughout this report.

Adjustment of Sphere Temperature Measurements

The reduced sphere temperatures from the telemetry output differed by approximately 12° R shortly after burnout. At this time, all sphere temperatures should have indicated approximately the saturation temperature corresponding to a sphere pressure of 15 pounds per square inch absolute because the hydrogen wetted the entire wall, as evidenced by the sharp decrease in temperature of the upper part of the sphere. Hence, each sphere temperature was adjusted by subtracting a constant temperature difference corresponding to its temperature after burnout minus 36.6° R, which is the saturation temperature for 15 pounds per square inch absolute. Subsequent rocket flight data have verified that the data as corrected above are valid.

Adjustment of Sphere Pressure

The reduced sphere pressures from telemetry are shown in figure 26 for pressures up to 50 pounds per square inch absolute. Two pressure gages were used, one for 0 to 50 and the other for 0 to 200 pounds per square inch absolute. At launch, the low-pressure gage read 14.7 and the high-pressure gage read about 12.5 pounds per square inch absolute. The two gages were of identical construction; therefore, the 50-pound-per-square-inch-absolute gage was more accurate in its range than the 200-pound-per-square-inch-absolute gage. For this reason and because of the 14.7-pound-per-square-inch-absolute reading at launch, the 50-pound-per-square-inch-absolute gage reading was accepted up to 48 pounds per square inch absolute. Beyond 48 pounds per square inch absolute, the high-pressure reading was multiplied by a constant factor of 1.14, which is the approximate ratio of the low-pressure gage reading to the high-pressure reading at 225 seconds. Subsequent rocket flight data have verified that the data as corrected are valid.

Estimate of Velocity Required for Forced Convection

Using the heat-transfer rate into the hydrogen (270 Btu/(hr)(sq ft)) and the approximate ΔT (about 1° R) gives the coefficient of heat transfer h_l.

$$h_l = \frac{\dot{Q}/A}{\Delta T} = 270 \frac{\text{Btu}}{(\text{hr})(\text{sq ft})(^\circ\text{R})}$$

A rough approximation of the velocity of the liquid required to transport 270 Btu per hour per square foot can be obtained from the following equation for flow through a pipe (ref. 21):

$$\frac{h_l}{C_{pb}G}\left(\frac{C_p\mu}{k}\right)_f^{2/3}\frac{0.023}{\left(\frac{DG}{\mu_f}\right)^{0.2}}$$

where, in the notation of reference 21,

C_p specific heat at constant pressure evaluated at film temperature, Btu/(lb)($^{\circ}$R)

C_{pb} specific heat at constant pressure, Btu/(lb)($^{\circ}$R)

D diameter, ft

G mass velocity (density × velocity)

k thermal conductivity, Btu/(hr)(ft)($^{\circ}$R)

μ viscosity, lb/(hr)(ft)

and subscript f denotes properties evaluated at film temperature. From the above equation and h_l = 270 Btu per hour per square foot per $^{\circ}$R the velocity required is 5.7 feet per second (properties evaluated at 70 lb/sq in. abs).

APPENDIX B

SYMBOLS

A	area, sq ft
a	acceleration, ft/sec^2
C_p	specific heat, Btu/lb
g_o	normal gravitational acceleration, 32.2 ft/sec^2
H	enthalpy, Btu/lb
h_v	heat of vaporization, Btu/lb
k	thermal conductivity, (Btu)(in.)/(hr)(sq ft)(^oR)
L	characteristic length, ft
l	length of conduction path, in.
M	molecular weight
N	number of lead wires
n	fraction of earth's gravitational field
n_*	fraction of earth's gravitational field at which external forces are equivalent to intermolecular forces
P	pressure, lb/sq in. abs
P_G	gage pressure, microns of mercury
p	percentage of liquid in sphere by volume
Q	heat, Btu
$\dot{Q}$	heat-transfer rate, Btu/hr
$\dot{Q}_{gc}$	heat transferred to hydrogen sphere by gaseous conduction, Btu/hr
$\dot{Q}_r$	heat transferred to hydrogen sphere by radiation from heater, Btu/hr

$\dot{Q}_{sc}$ heat transferred to hydrogen sphere by solid conduction, Btu/hr

q heat added to constant volume system, Btu/lb

T temperature, ^{o}R

T_G temperature at gage that measures P_G, ^{o}R

t time, hr

V volume, cu ft

v specific volume, (Container volume)/(Total mass of liquid and vapor), cu ft/lb

W weight of hydrogen containment sphere, lb

α accommodation coefficient

γ ratio of specific heats

ϵ total hemispherical emissivity

ρ density, lb/cu ft

σ Stefan-Boltzmann constant, 0.1713×10^{-8} Btu/(hr)(ft^2)($^{o}R^4$)

σ_{st} surface tension, lb/ft

Subscripts:

abs absorbed

avg average

bo boiloff

Cu copper

c camera port

f-v fill-vent tubes

h heater

ilt	instrumentation lead tube
L	lead wires
s	hydrogen sphere wall
sc	solid conduction
sl	saturated liquid
sr	support ring
ss	stainless steel
sv	saturated vapor
w	inner surface of nitrogen cooling jacket

REFERENCES

1. Benedikt, E. T.: General Behavior of a Liquid in a Zero or Near Zero Gravity Environment. ASG-TM-60-9Z6, Norair Div., Northrop Corp., May 1960.

2. Li, Ta: Liquid Behavior in a Zero-G Field. AE-60-0682, Convair Astronautics, Aug. 1960.

3. Li, Ta: Cryogenic Liquids in the Absence of Gravity. Paper presented at 1961 Cryogenic Eng. Conf., Ann Arbor (Mich.), Aug. 1961.

4. Petrash, Donald A., Zappa, Robert F., and Otto, Edward W.: Experimental Study of the Effects of Weightlessness on the Configuration of Mercury and Alcohol in Spherical Tanks. NASA TN D-1197, 1962.

5. Reynolds, William C.: Behavior of Liquids in Free Fall. Jour. Aero/Space Sci., vol. 26, no. 12, Dec. 1959, pp. 847-848.

6. Neu, J. T., Ferriso, C. C., and Boynton, F. P.: Condition of Liquid Hydrogen Under Zero G. AZJ-55-002, Convair Astronautics, Feb. 6, 1959.

7. Trusela, Robert A., and Clodfelter, Robert G.: Heat Transfer Problems of Space Vehicle Power Systems. Paper 154C, SAE, Inc., 1960.

8. Westwater, J. W.: Things We Don't Know About Boiling Heat Transfer. Dept. Chem. and Chem. Eng., Univ. Ill.

9. Zuber, Novak, and Fried, Erwin: Two-Phase Flow and Boiling Heat Transfer to Cryogenic Liquids. Paper 1709-61, Am. Rocket Soc., Inc., 1961.

10. Merte, H., and Clark J. A.: Boiling Heat Transfer Data for Liquid Nitrogen at Standard and Near Zero-Gravity. Paper presented at 1961 Cryogenic Eng. Conf., Ann Arbor (Mich.), Aug. 1961.

11. Aerophysics Group: June-August Progress Report for the Combined Laboratory and KC-135 Aircraft Zero-G Test Program. Rep. AE61-0871, Convair Astronautics, Sept. 5, 1961.

12. Usiskin, C. M., and Siegel, R.: An Experimental Study of Boiling in Reduced and Zero Gravity Fields. Paper 60-HT-10, ASME-AIChE, 1960.

13. Steinle, H. F., and Schwartz, E. W.: An Experimental Study of the Transition from Nucleate to Film Boiling Under Zero Gravity Conditions. AZJ-55-009, Convair Astronautics, Nov. 23, 1959.

14. Class, C. R., DeHaan, J. R., Piccone, M., and Cost, R. B.: Boiling Heat Transfer to Liquid Hydrogen from Flat Surfaces. Vol. 5 of Advances in Cryogenic Eng., Plenum Press, 1959, pp. 254-261.

15. Drayer, D. E., and Timmerhaus, K. D.: An Experimental Investigation of the Individual Boiling and Condensing Heat Transfer Coefficients for Hydrogen. Paper presented at 1961 Cryogenic Eng. Conf., Ann Arbor (Mich.), Aug. 1961.

16. Malkov, M. P., Zeldovitch, A. G., Fradkov, A. B., and Danilov, I.B.: Industrial Separation of Deuterium by Low-Temperature Distillation. Proc. Second United Nations Int. Conf. on Peaceful Uses of Atomic Energy, vol. 4, 1958, pp. 491-498.

17. Scott, L. E., Robbins, R. F., Mann, D. B., and Birmingham, B. W.: Temperature Stratification in a Nonventing Liquid Helium Dewar. Jour. Res. Nat. Bur. Standards, vol. 64C, no. 1, Jan.-Mar., 1960, pp. 19-23.

18. Huntley, Sidney C.: Temperature-Pressure-Time Relations in a Closed Cryogenic Container. NACA TN 4259, 1958.

19. Scott, Russell, B.: Cryogenic Engineering. D. Van Nostrand Co., Inc. 1959.

20. Goodwin, R. D., et al.: Provisional Thermodynamic Functions for Para Hydrogen. Rep. 6791, NBS, Aug. 4, 1961.

21. McAdams, William H.: Heat Transmission. Third ed., McGraw-Hill Book Co., Inc., 1954.

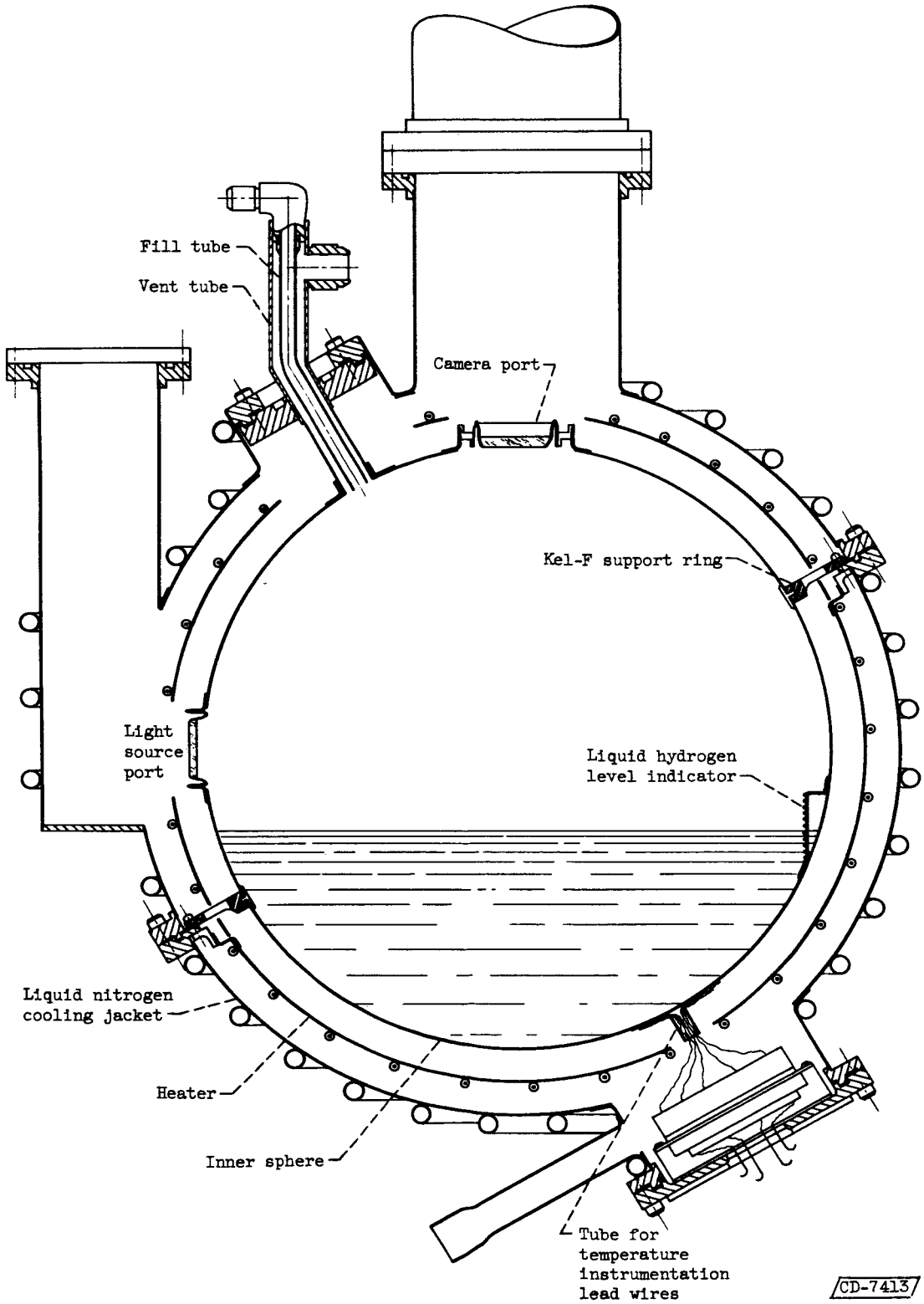

Figure 1. - Sketch of zero-gravity heat-transfer apparatus.

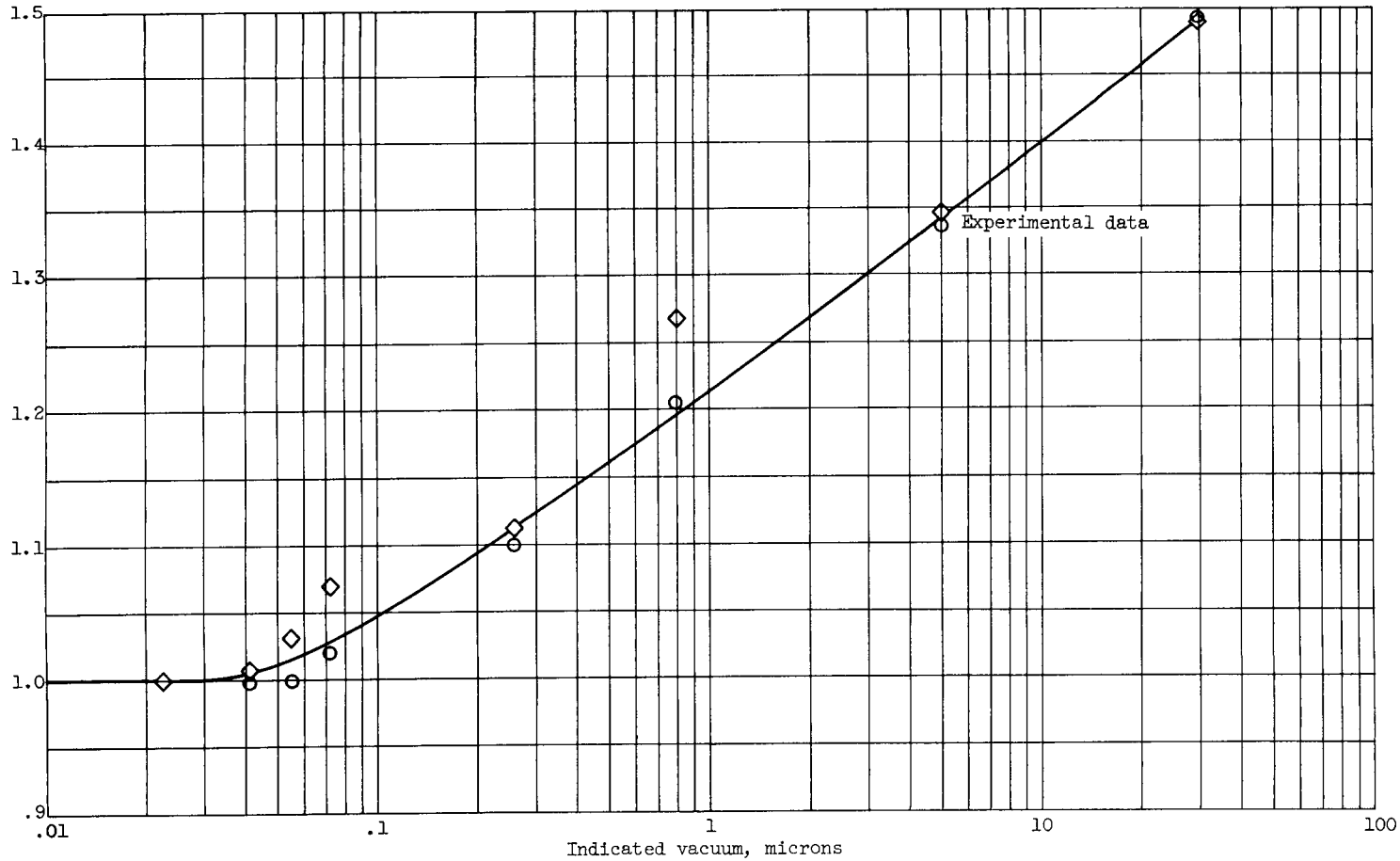

Figure 2. - Effect of vacuum on heat transfer. Nominal heat flux, 160 Btu per hour per square foot.

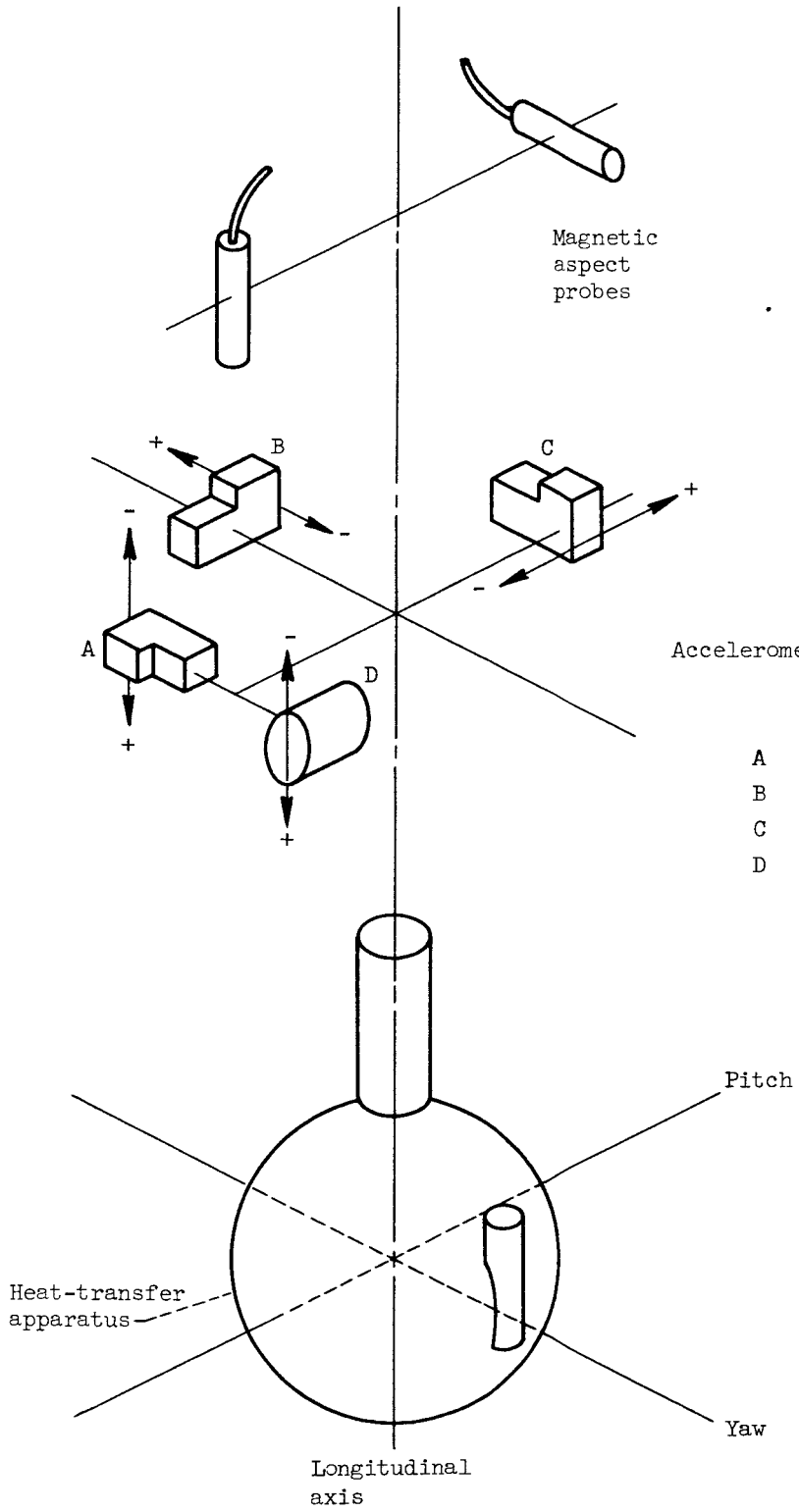

Accelerometers	Full-scale range, g
A	$\pm 10^{-2}$
B	$\pm 10^{-2}$
C	$\pm 10^{-2}$
D	$\pm 10^{-3}$

Figure 3. - Oriented instruments.

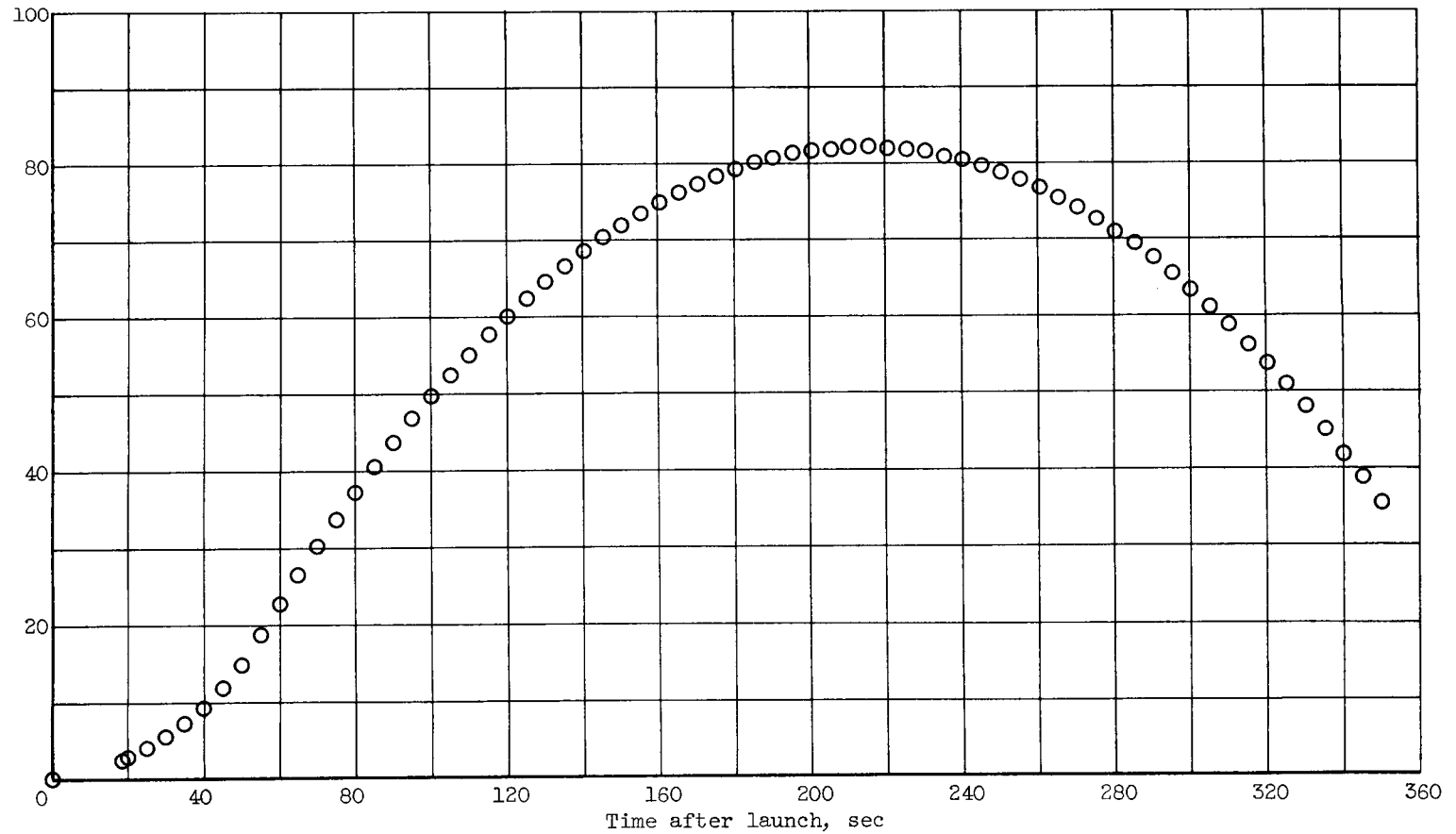

(a) Altitude.

Figure 4. - Trajectory parameters.

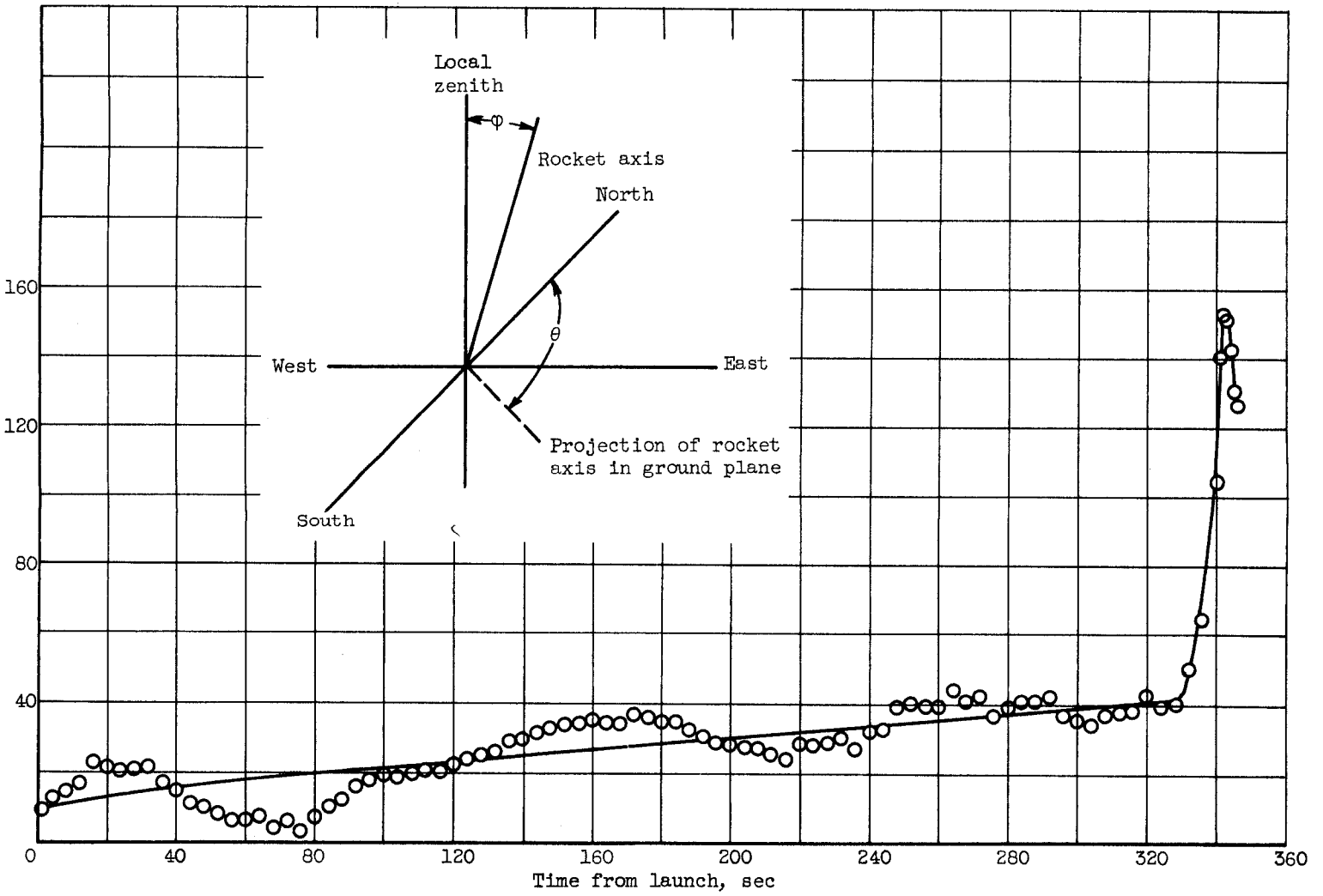

(b) Angle φ.

Figure 4. - Continued. Trajectory parameters.

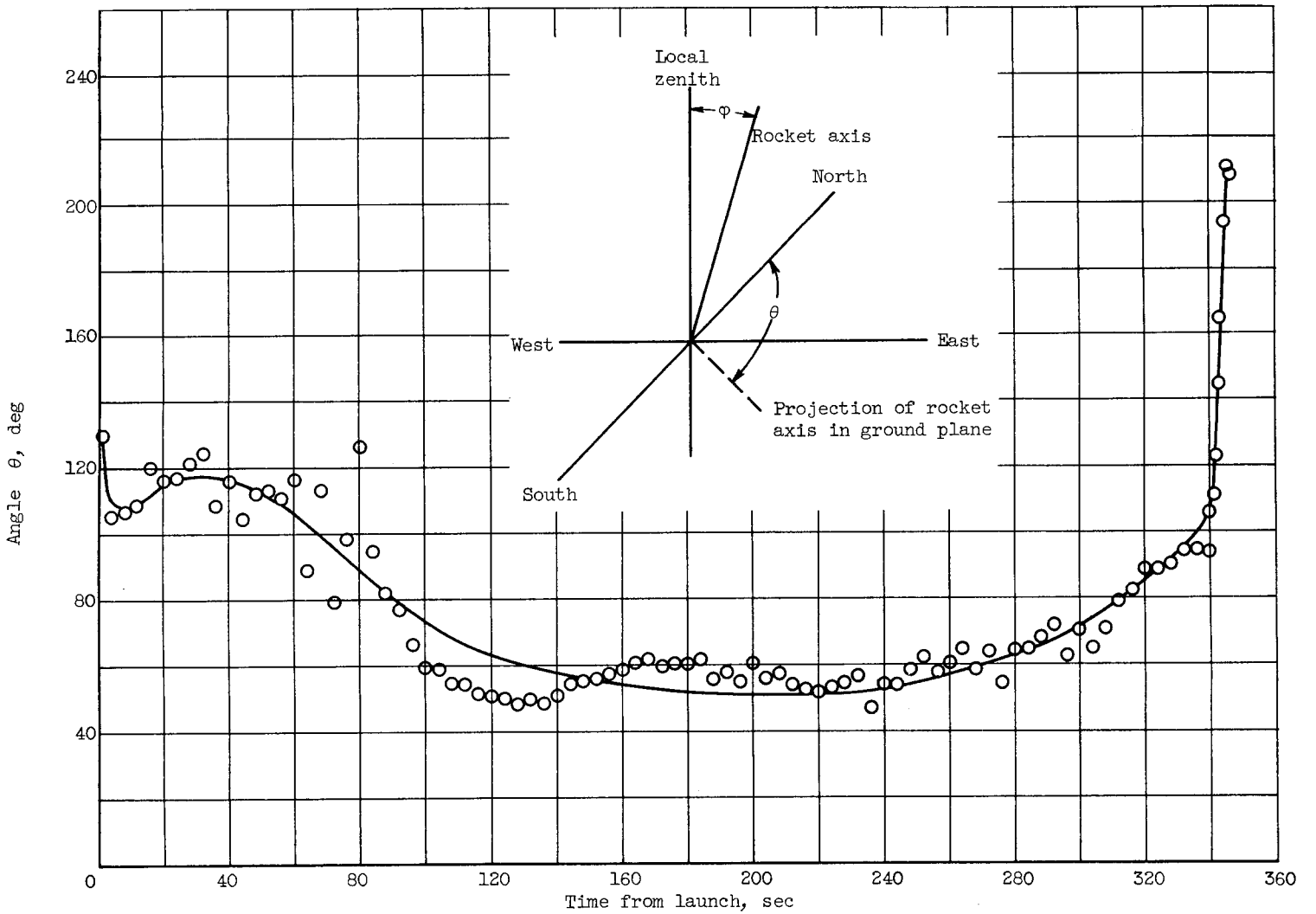

(c) Angle θ.

Figure 4. - Concluded. Trajectory parameters.

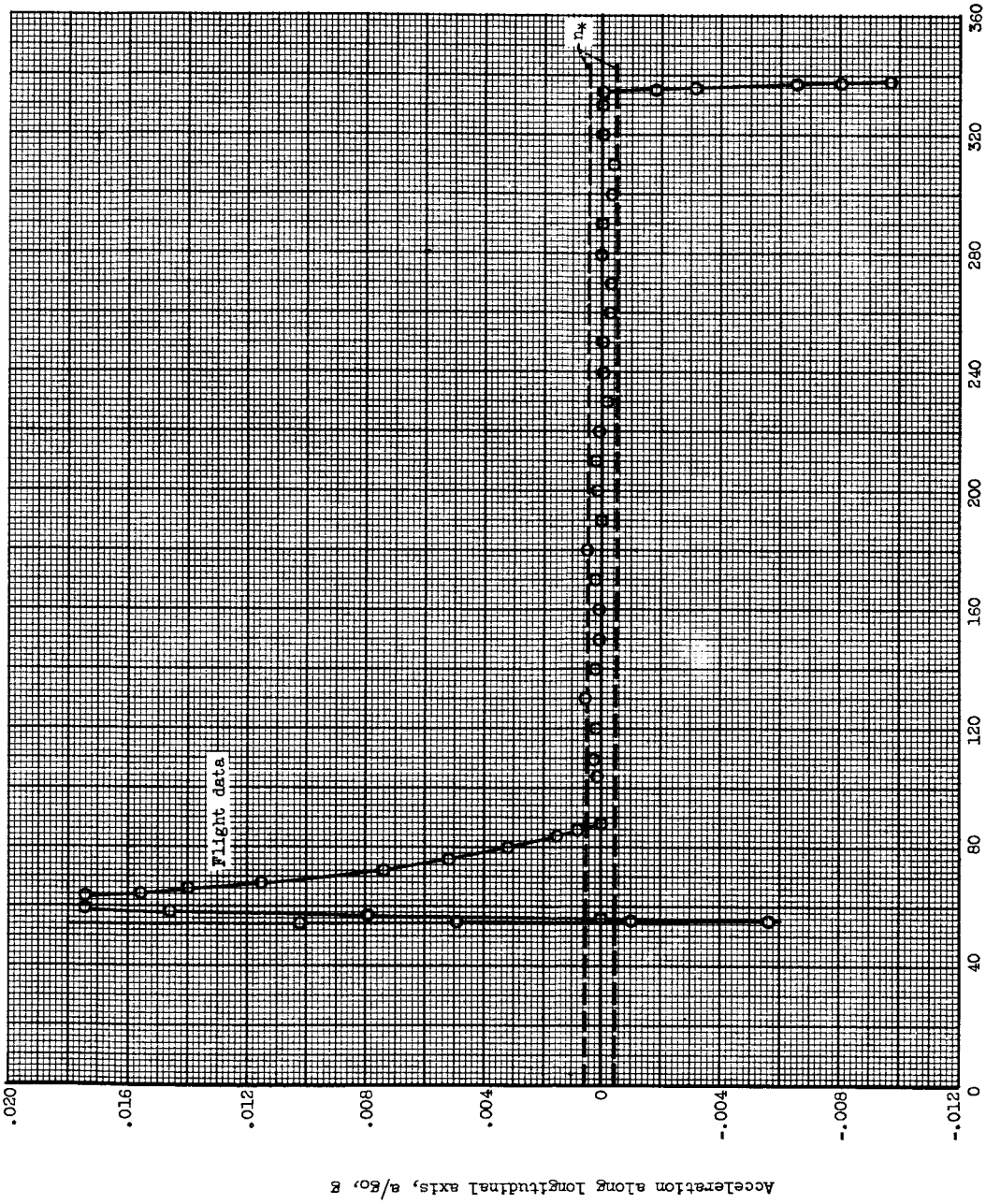

(a) Longitudinal axis.

Figure 5. - Acceleration during flight.

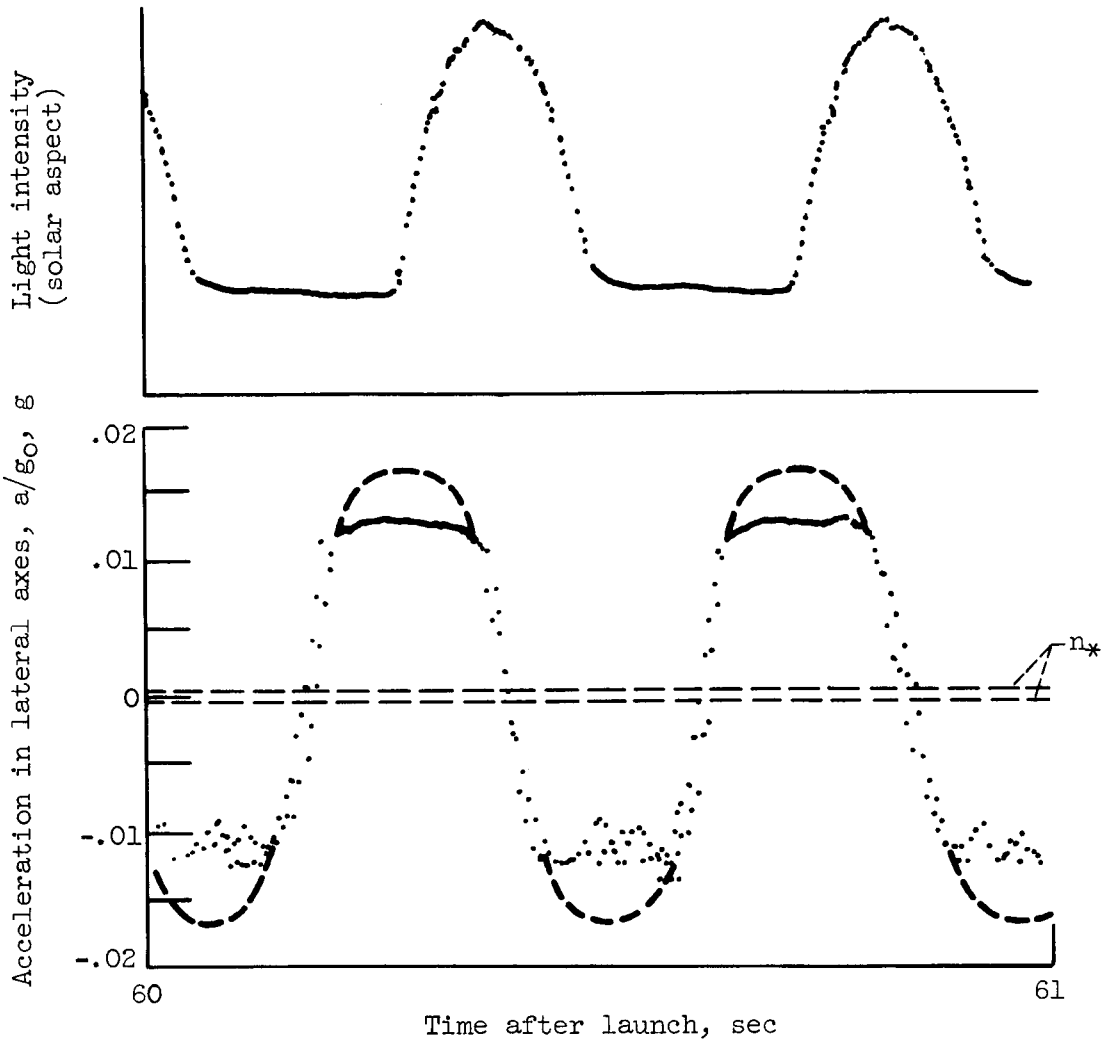

(b) Lateral axis and relation to light intensity from solar aspect indicators.

Figure 5. - Concluded. Acceleration during flight.

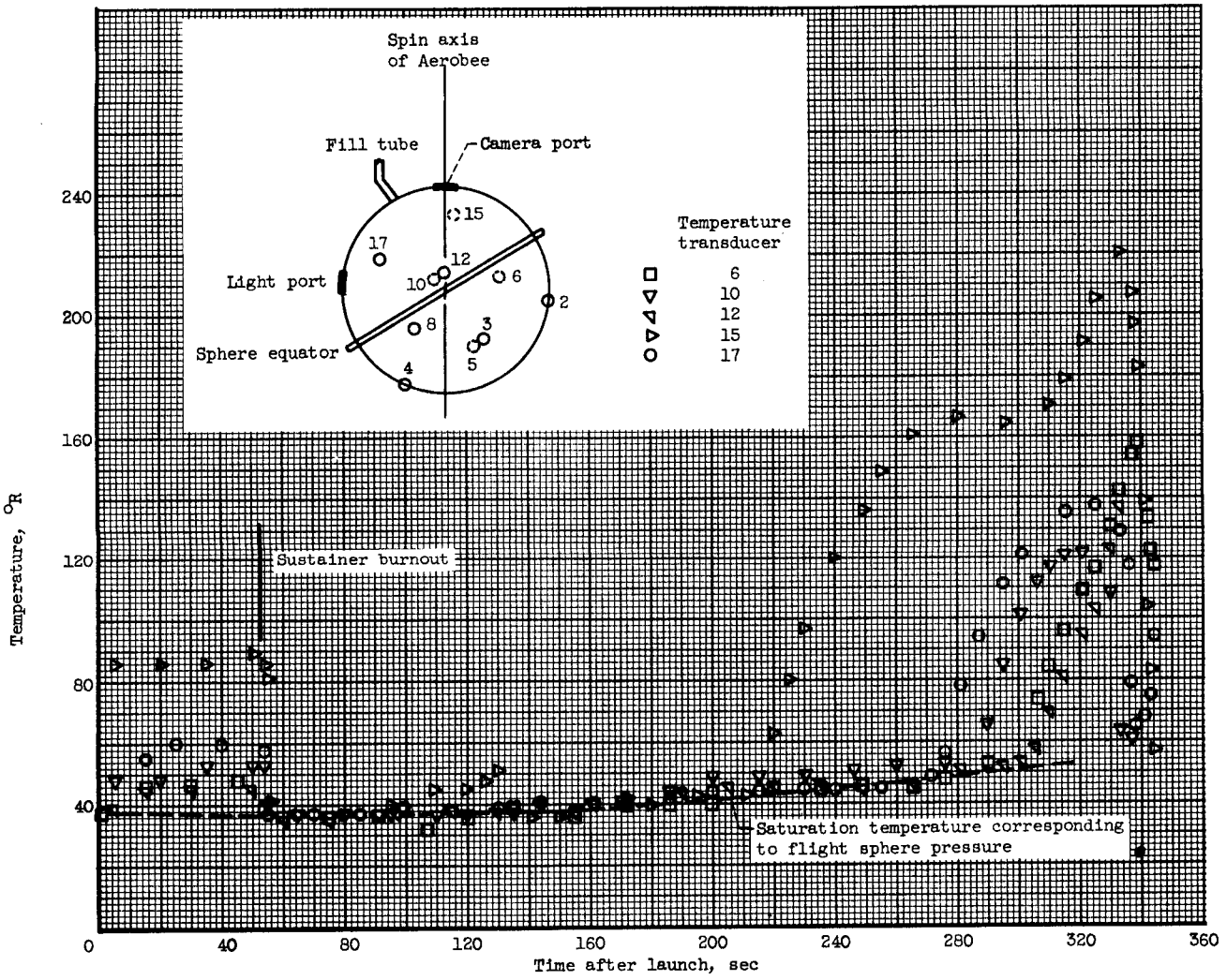

(a) Temperature transducers 6, 10, 12, 15, and 17.

Figure 6. - Sphere temperatures during flight.

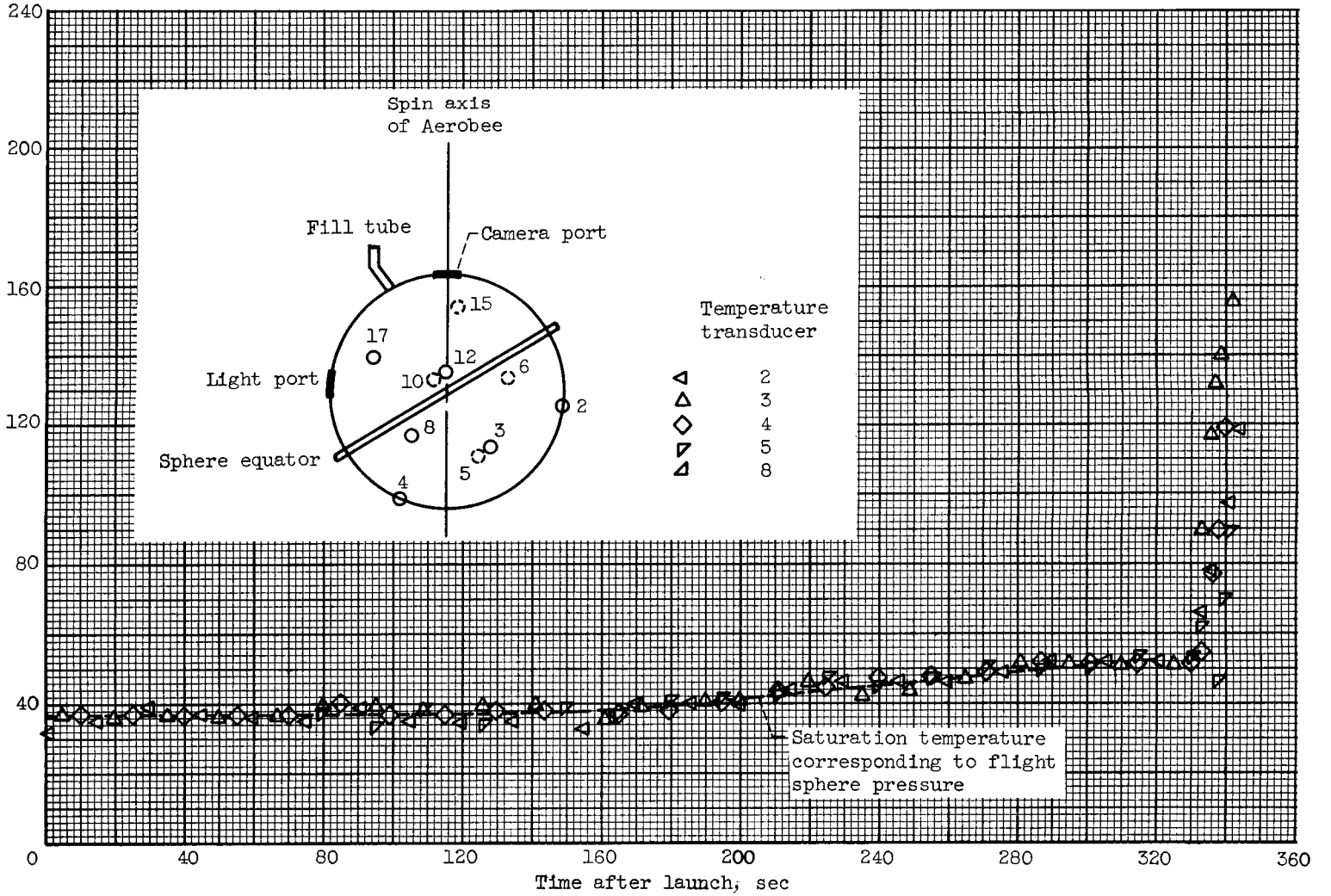

(b) Temperature transducers 2, 3, 4, 5, and 8.

Figure 6. - Concluded. Sphere temperatures during flight.

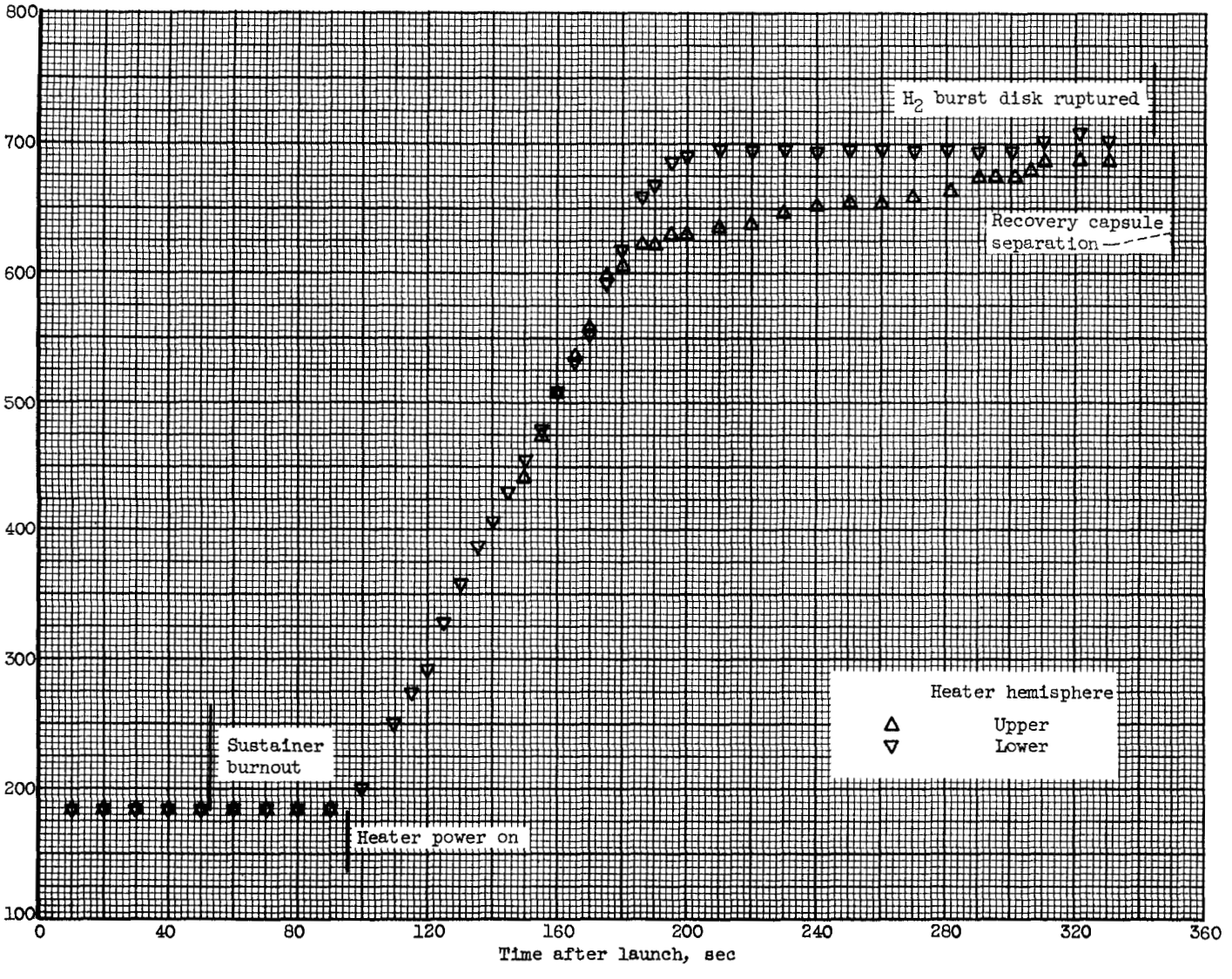

Figure 7. - Heater temperature during flight.

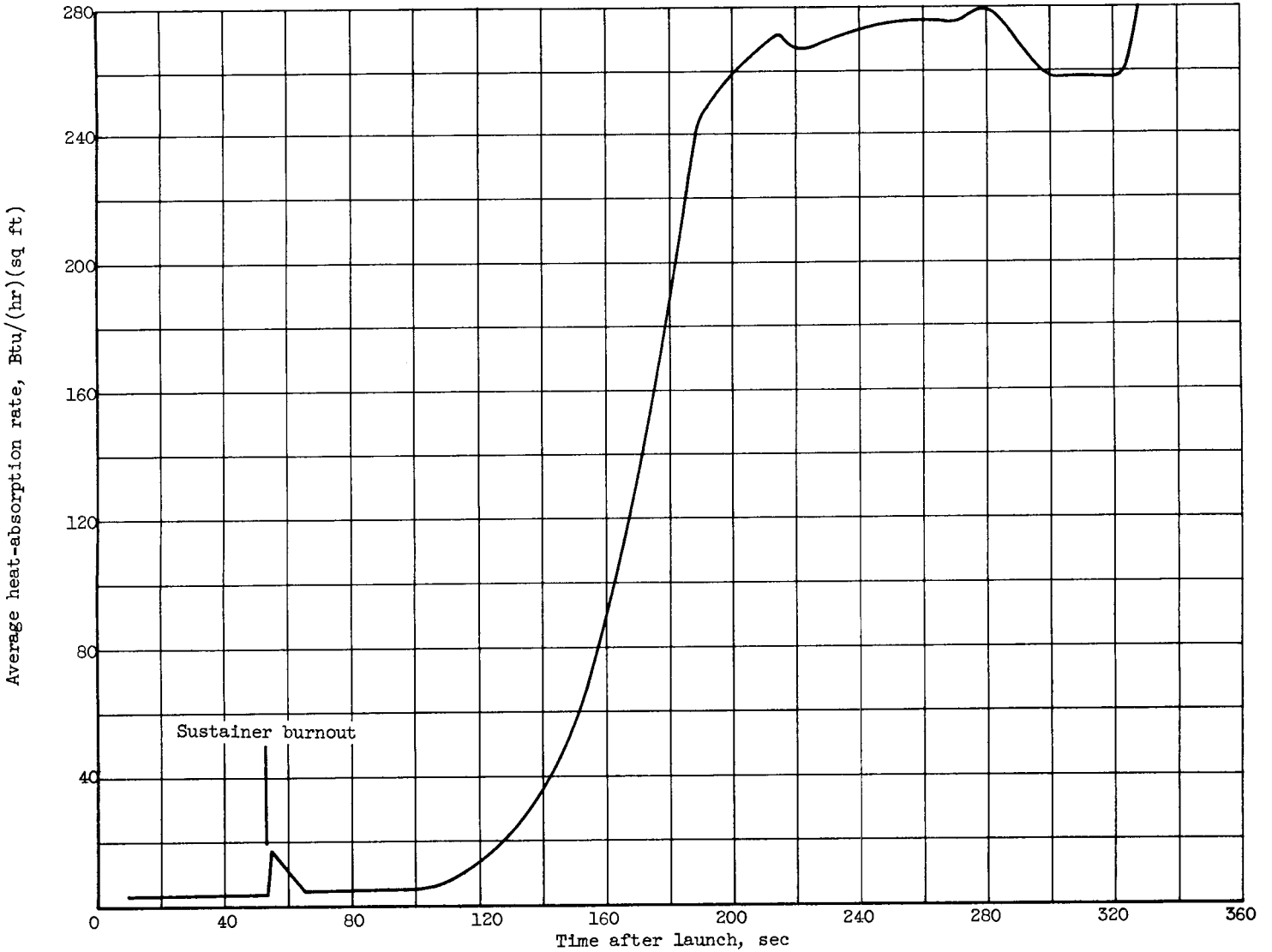

Figure 8. - Variation of heat-absorption rate by hydrogen during flight.

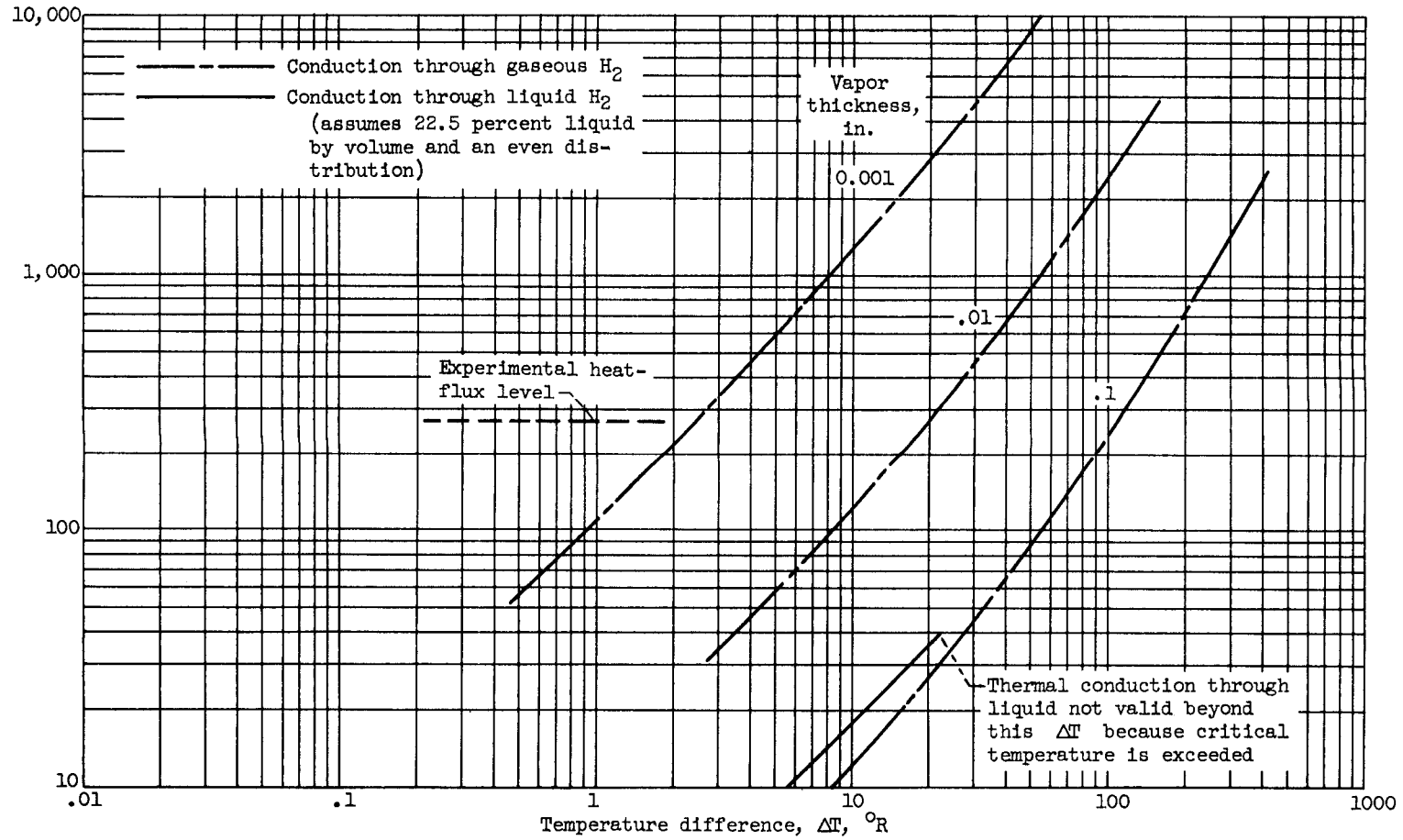

Figure 9. - Effect of temperature difference on thermal conduction.

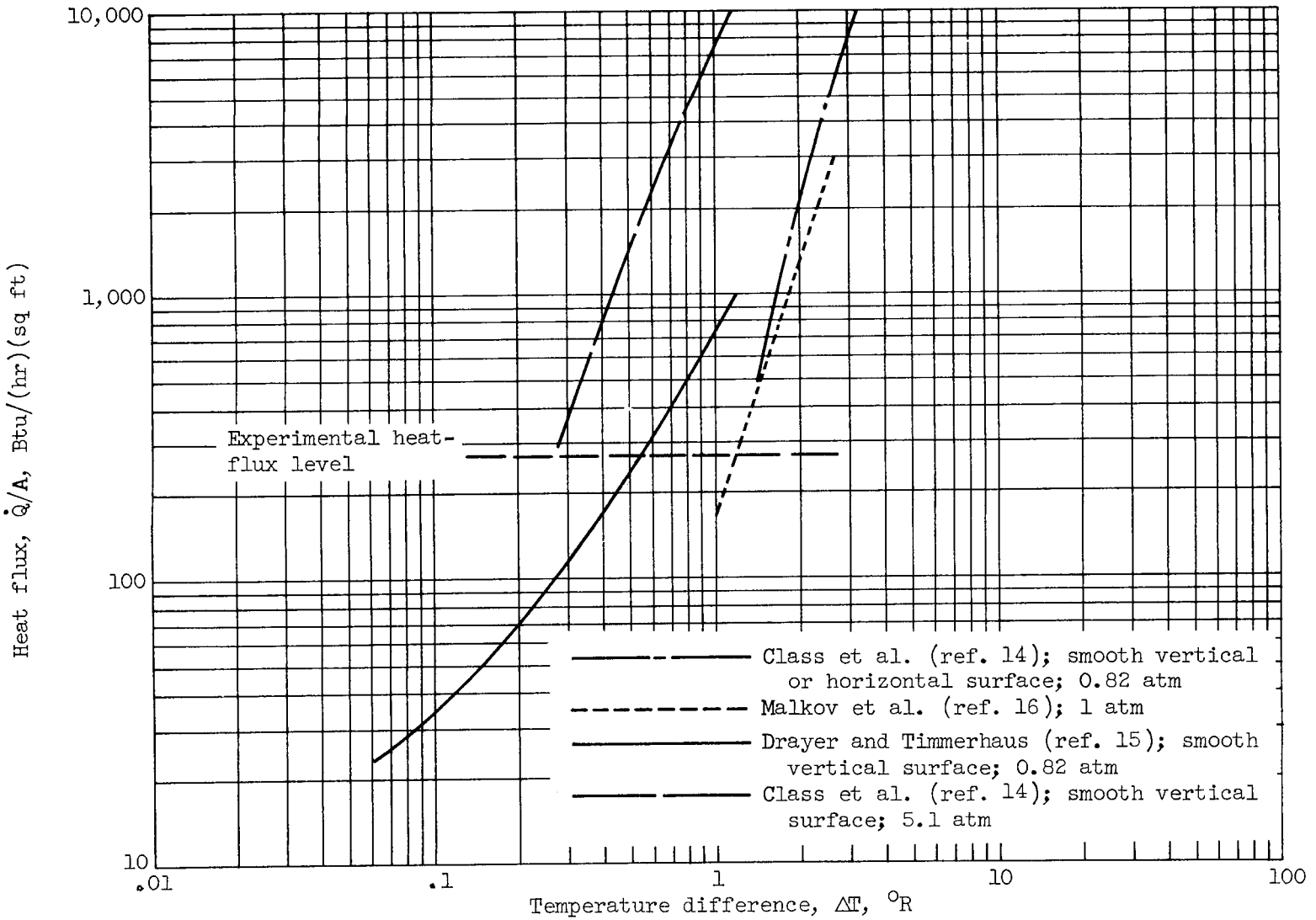

Figure 10. - Typical nucleate boiling data for liquid hydrogen.

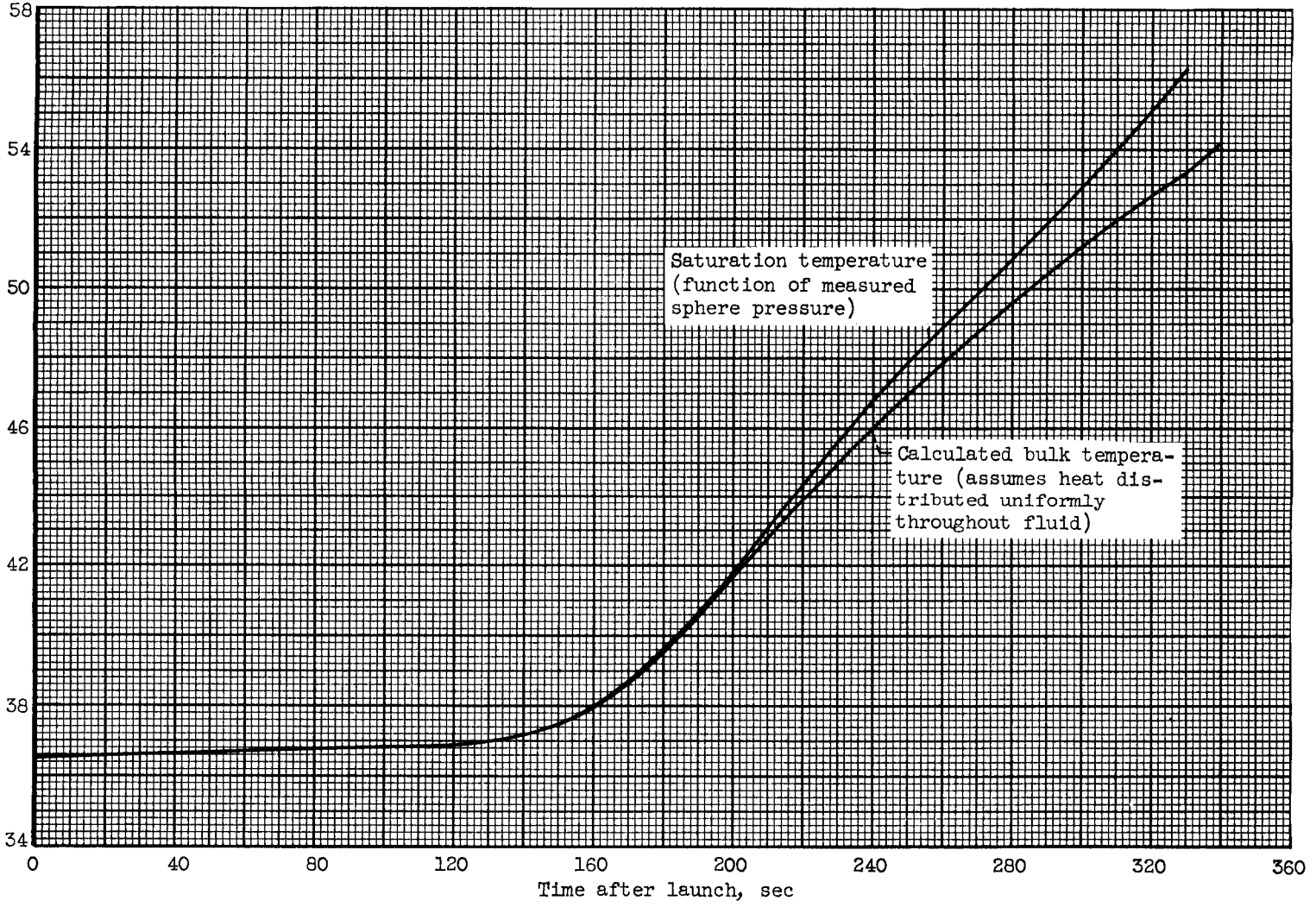

Figure 11. - Relation between saturation temperature and calculated bulk temperature.

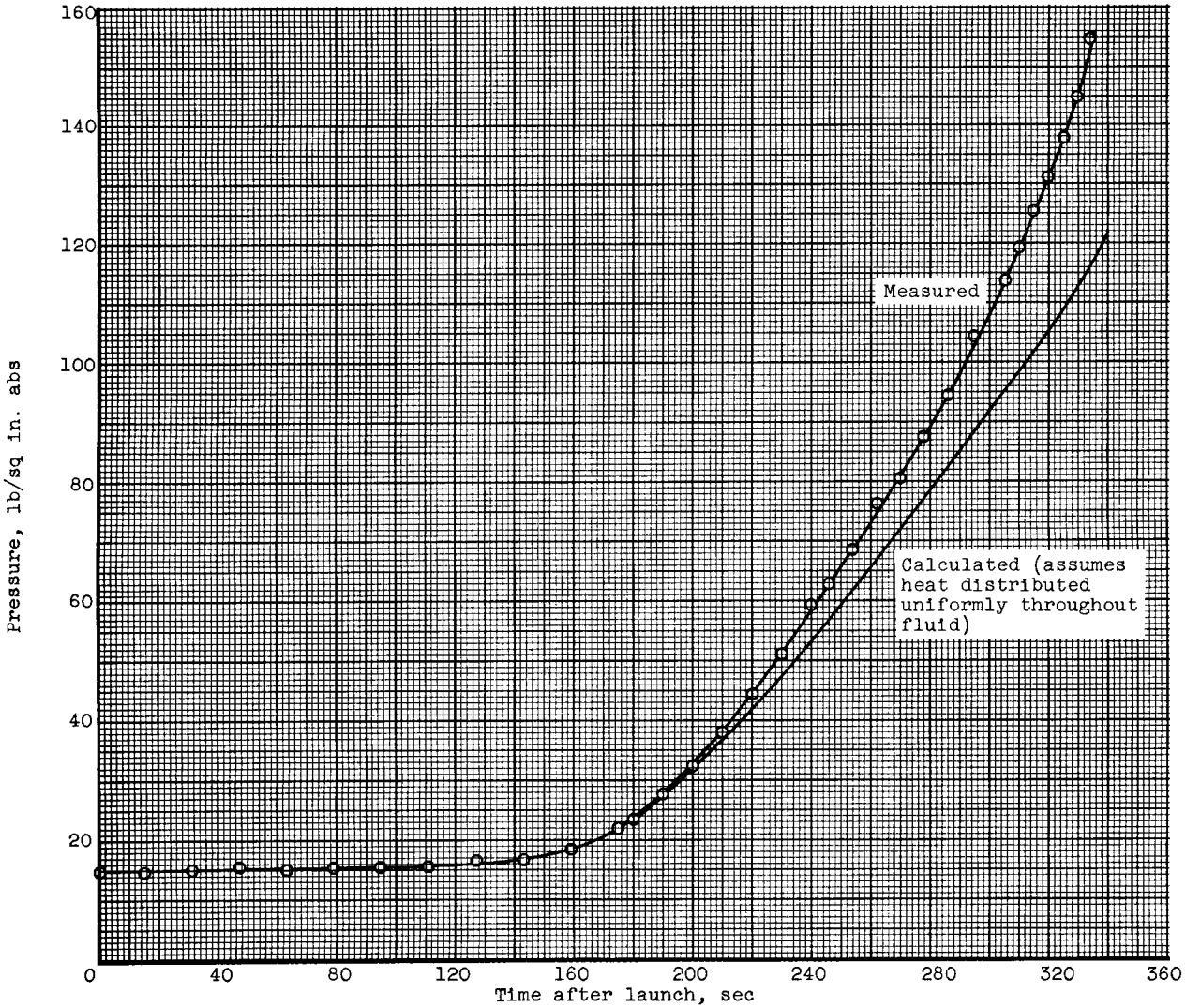

Figure 12. - Comparison of actual pressure during flight to calculated thermal equilibrium pressure.

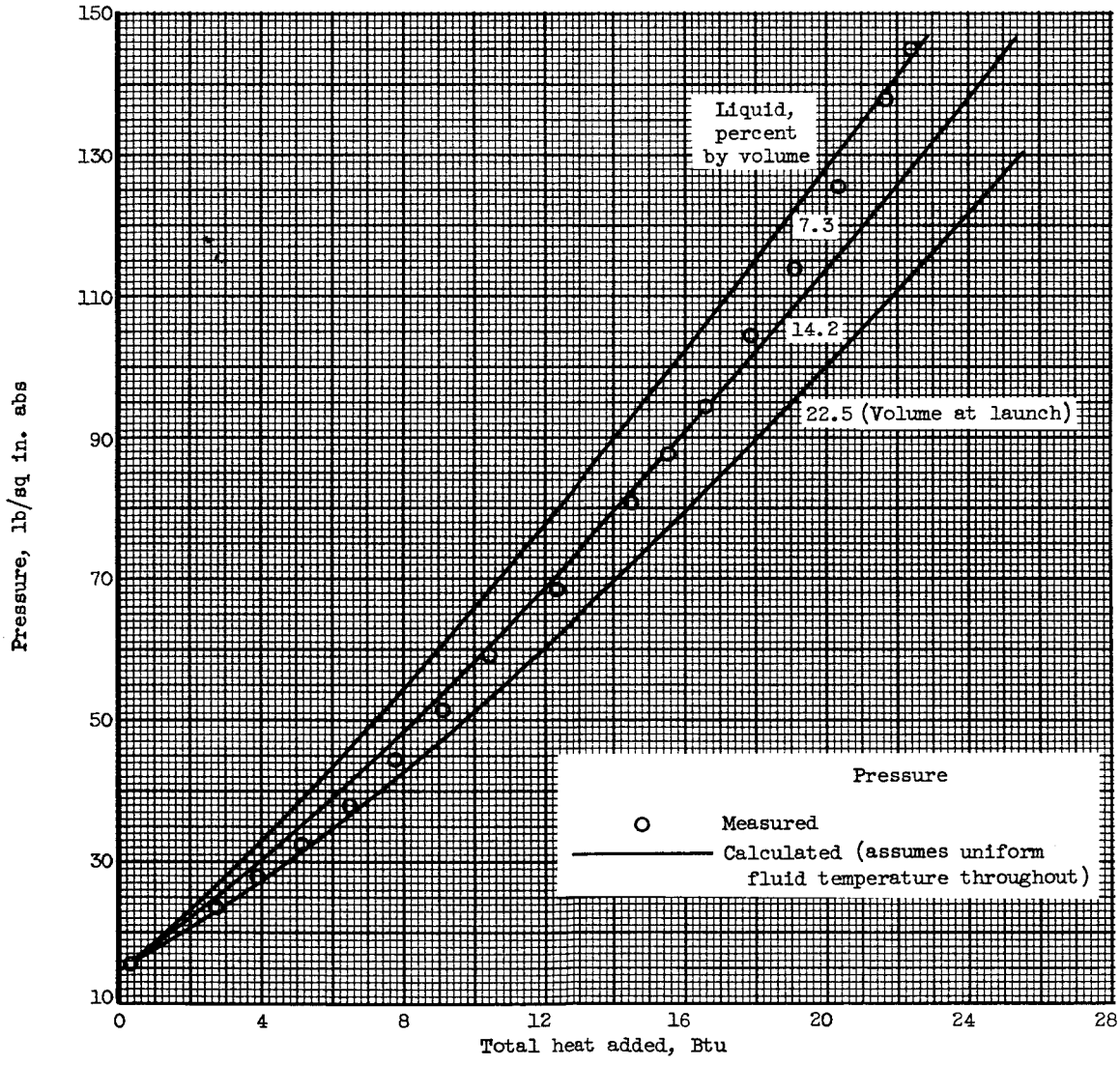

Figure 13. - Comparison of actual pressure and calculated thermal equilibrium pressure as function of total heat input.

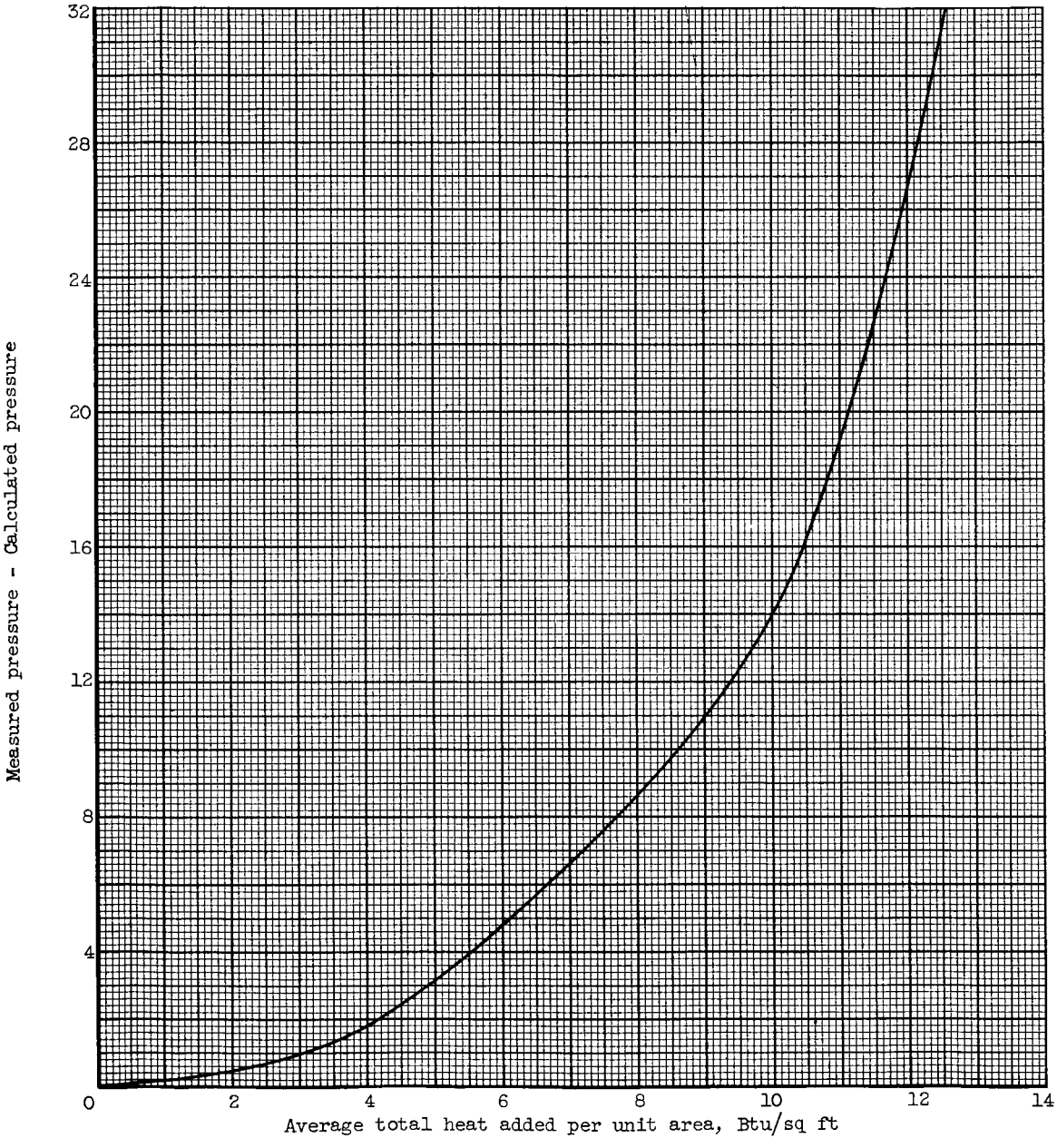

Figure 14. - Pressure difference as function of total heat added per unit area.

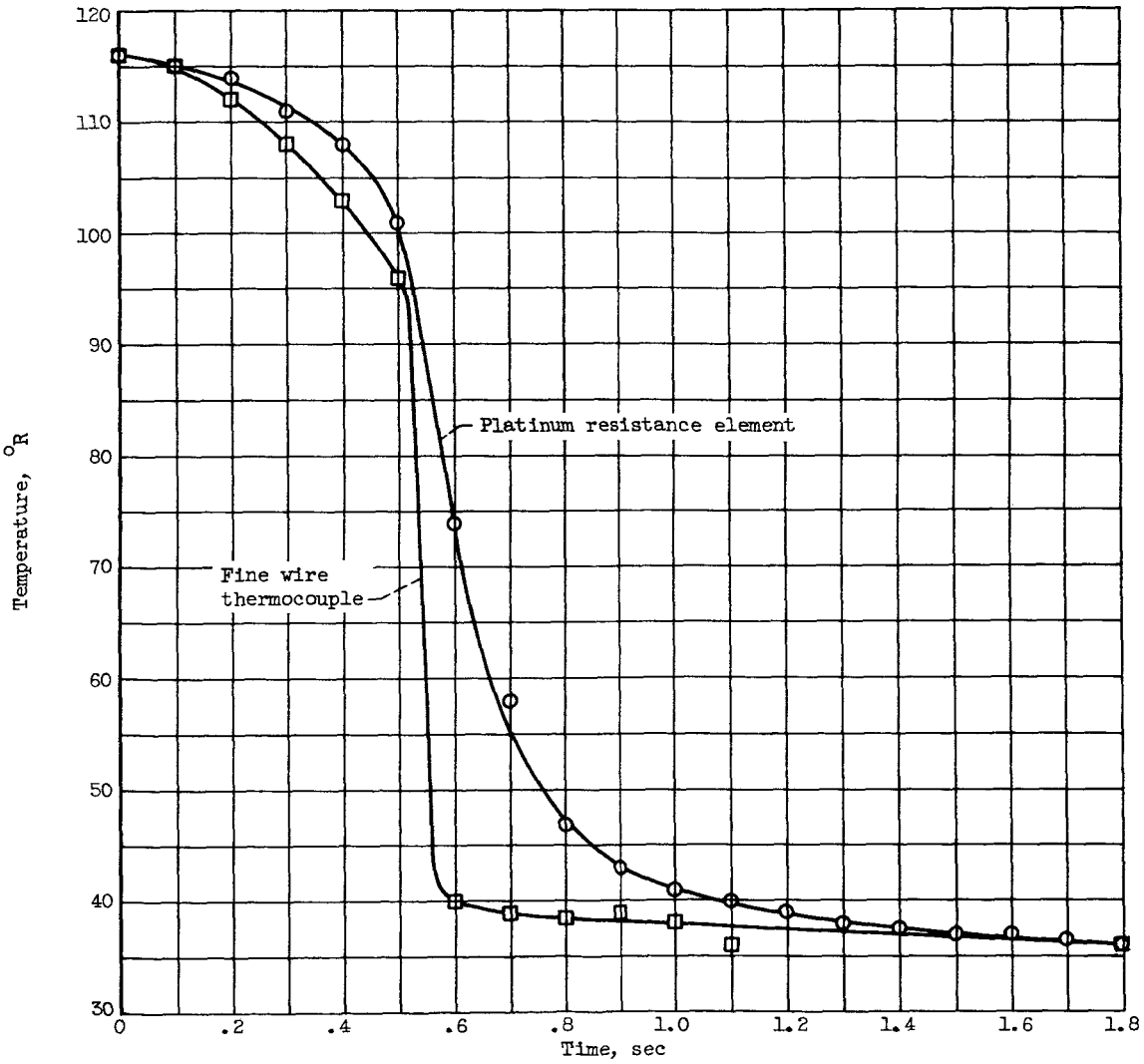

Figure 15. - Response of platinum resistance element and fine wire thermocouple to sudden insertion of 0.010-inch AM350 wall into liquid hydrogen. Wall initially wetted by hydrogen vapor; platinum resistance element and thermocouple on vacuum side of wall.

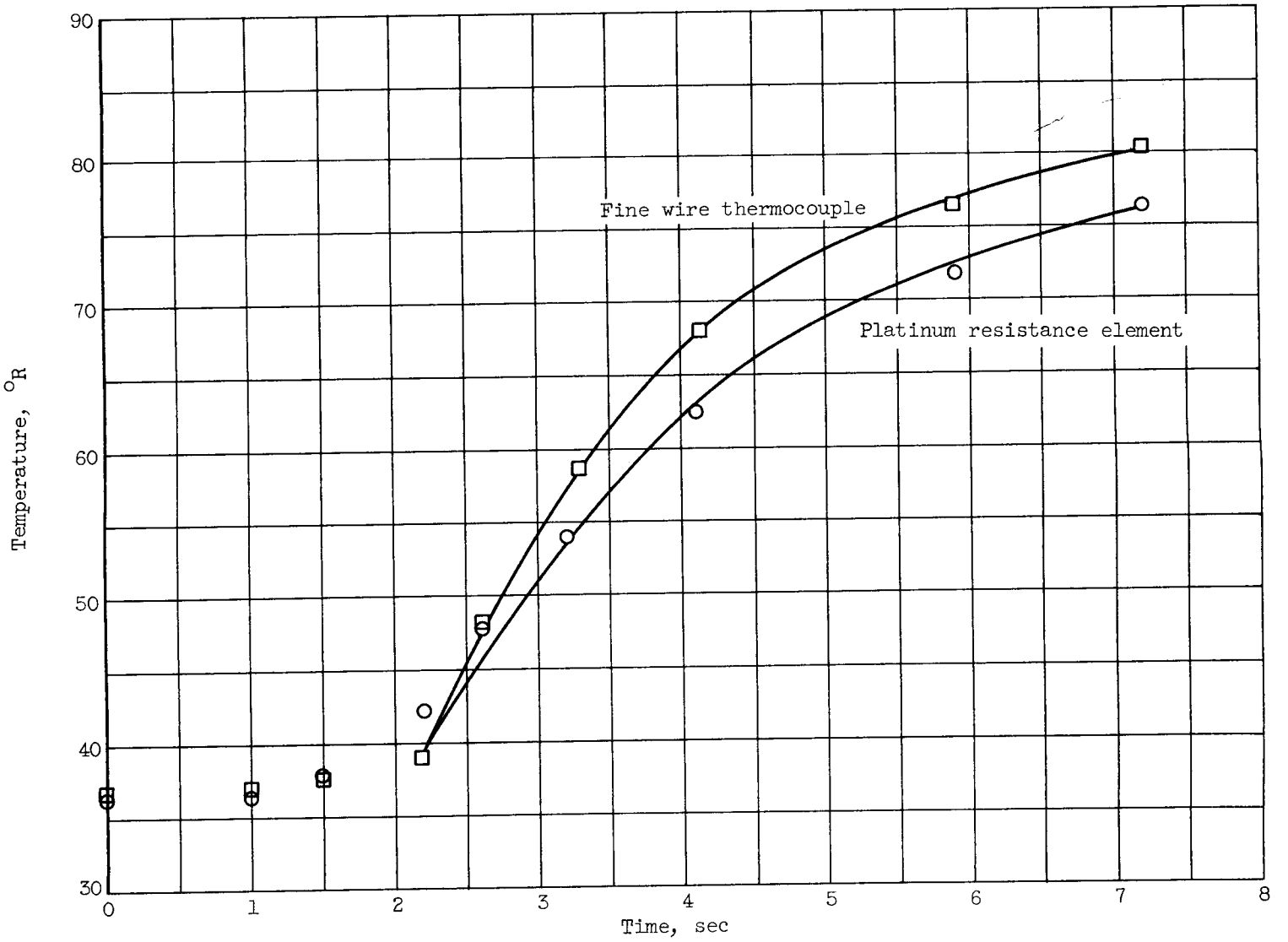

Figure 16. - Response of platinum resistance temperature transducer to increasing wall temperature.

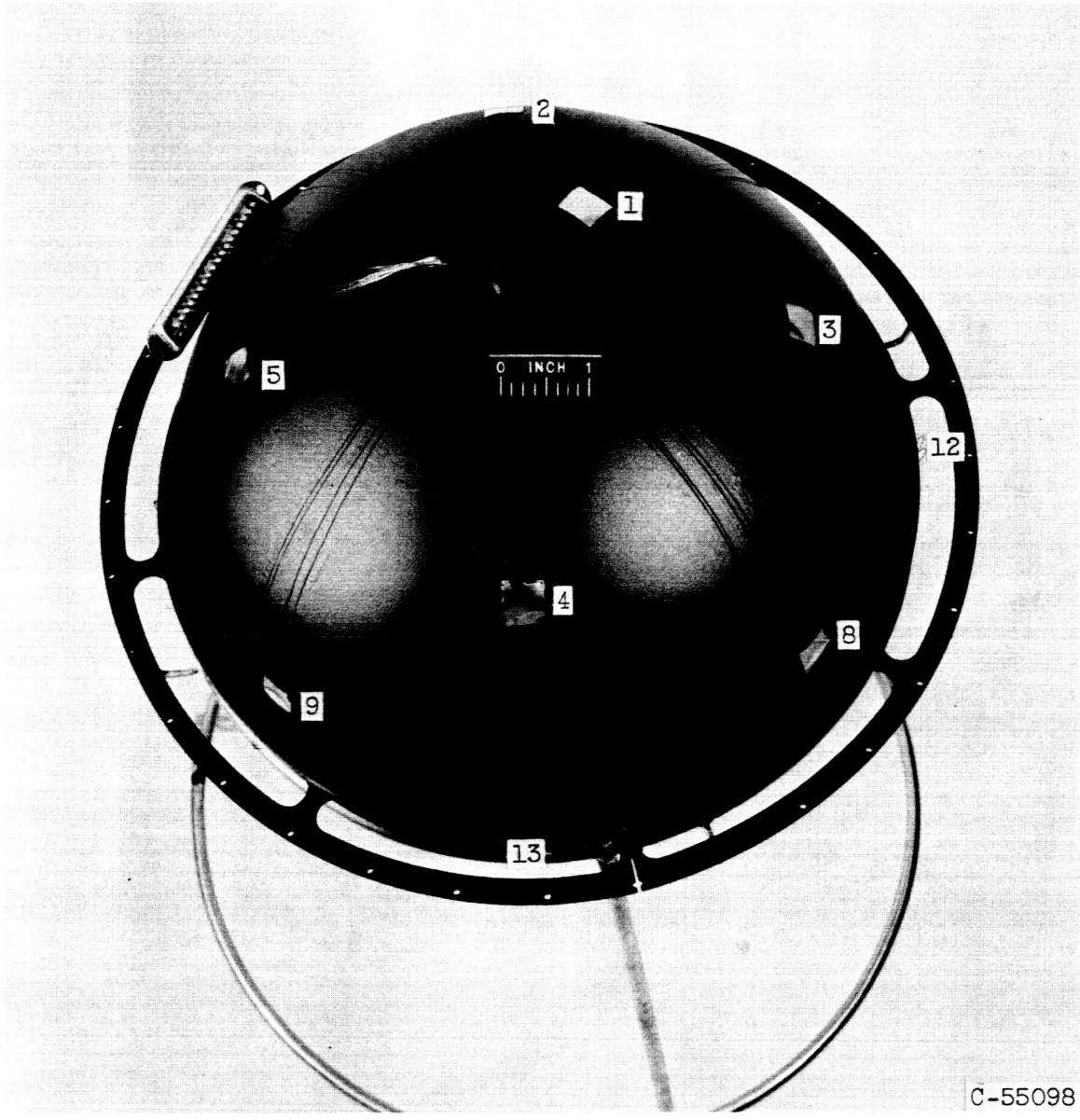

(a) Lower half of sphere.

Figure 17. - Location of temperature transducers on hydrogen sphere.

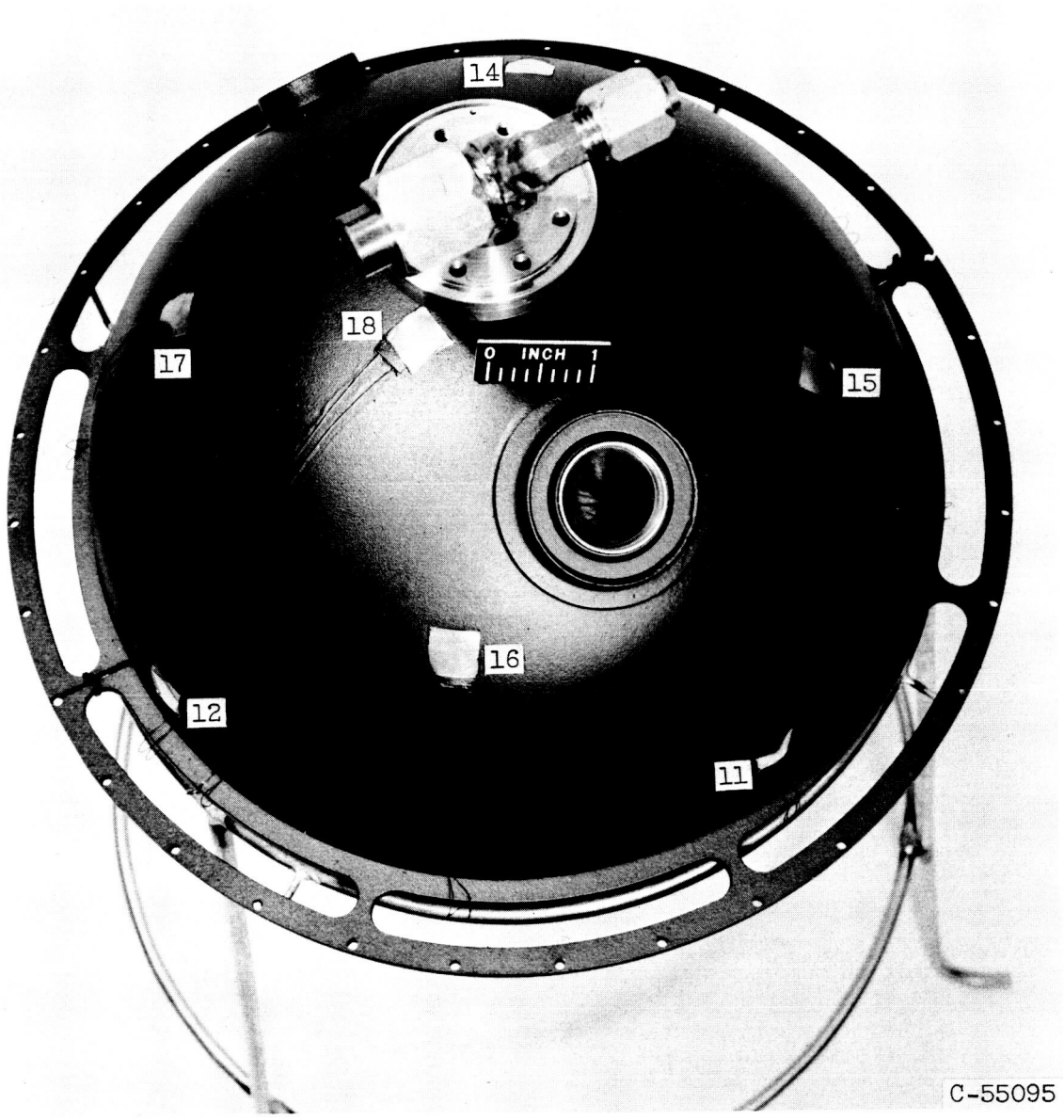

(b) Upper half of sphere.

Figure 17. - Continued. Location of temperature transducers on hydrogen sphere.

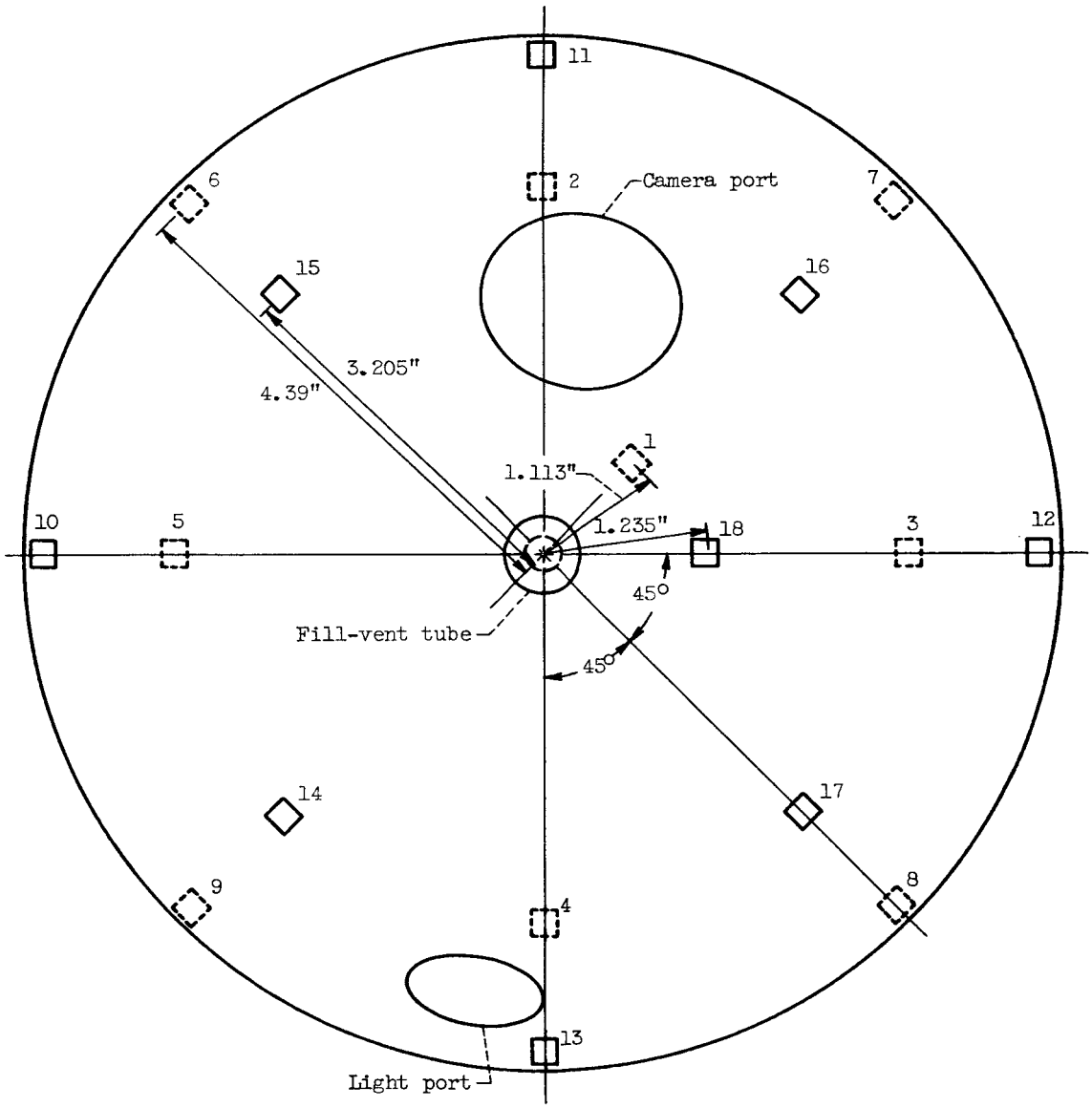

(c) Sketch. Note: Distances shown are those projected on plane of equator.

Figure 17. - Concluded. Location of temperature transducers on hydrogen sphere.

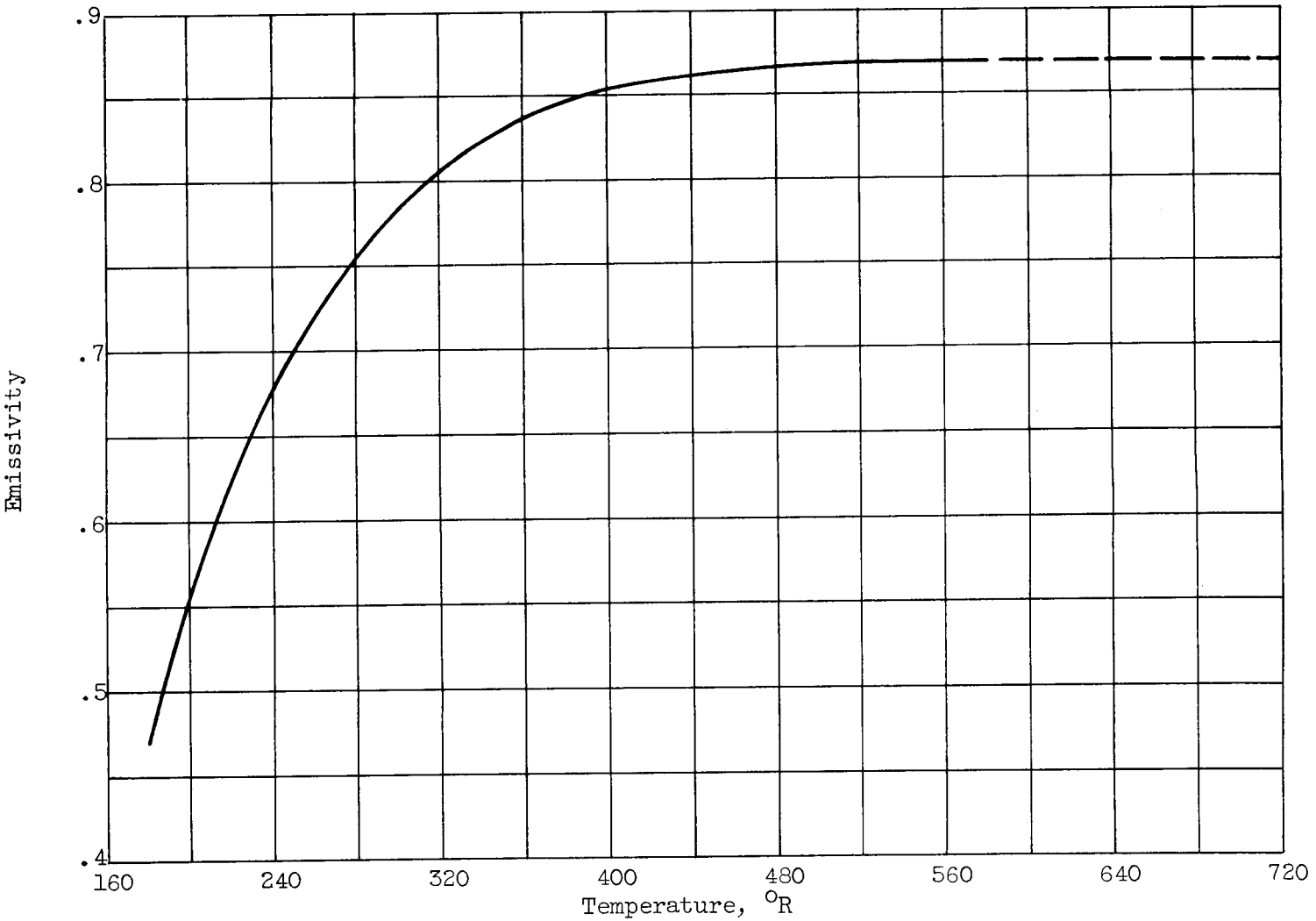

Figure 18. - Emissivity of heater and sphere as function of heater temperature.

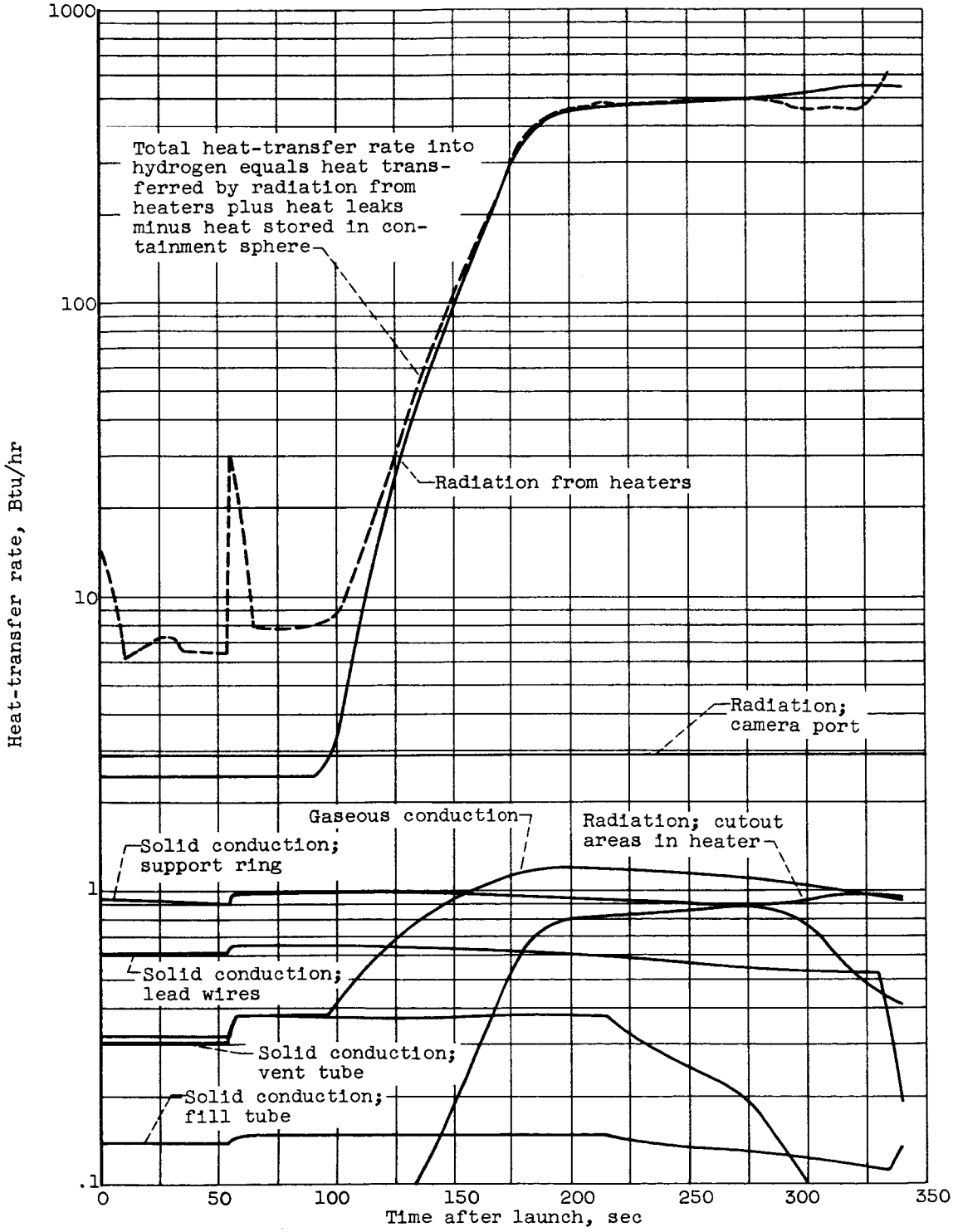

Figure 19. - History of heat-transfer rates during flight.

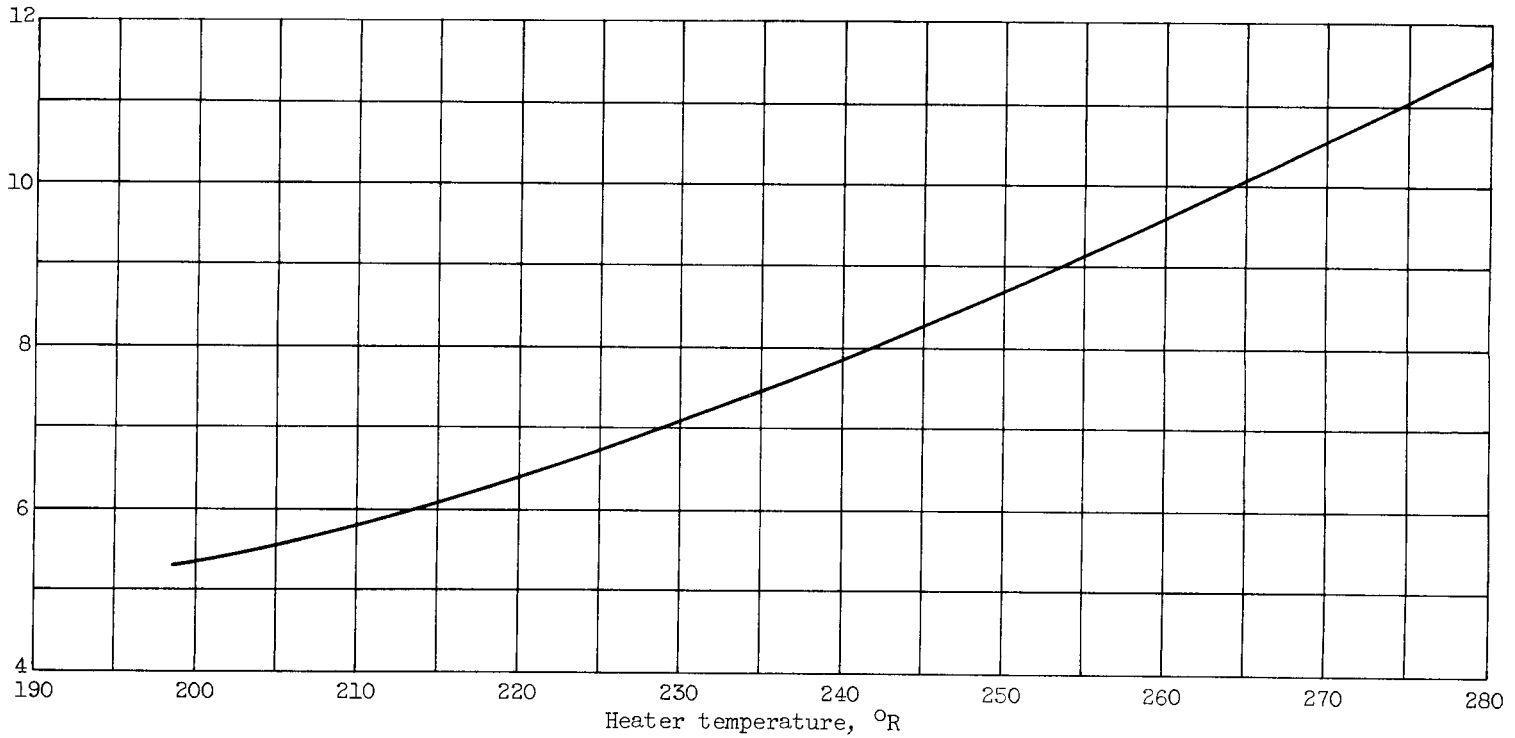

Figure 20. - Heat-leak rate as function of heater temperature.

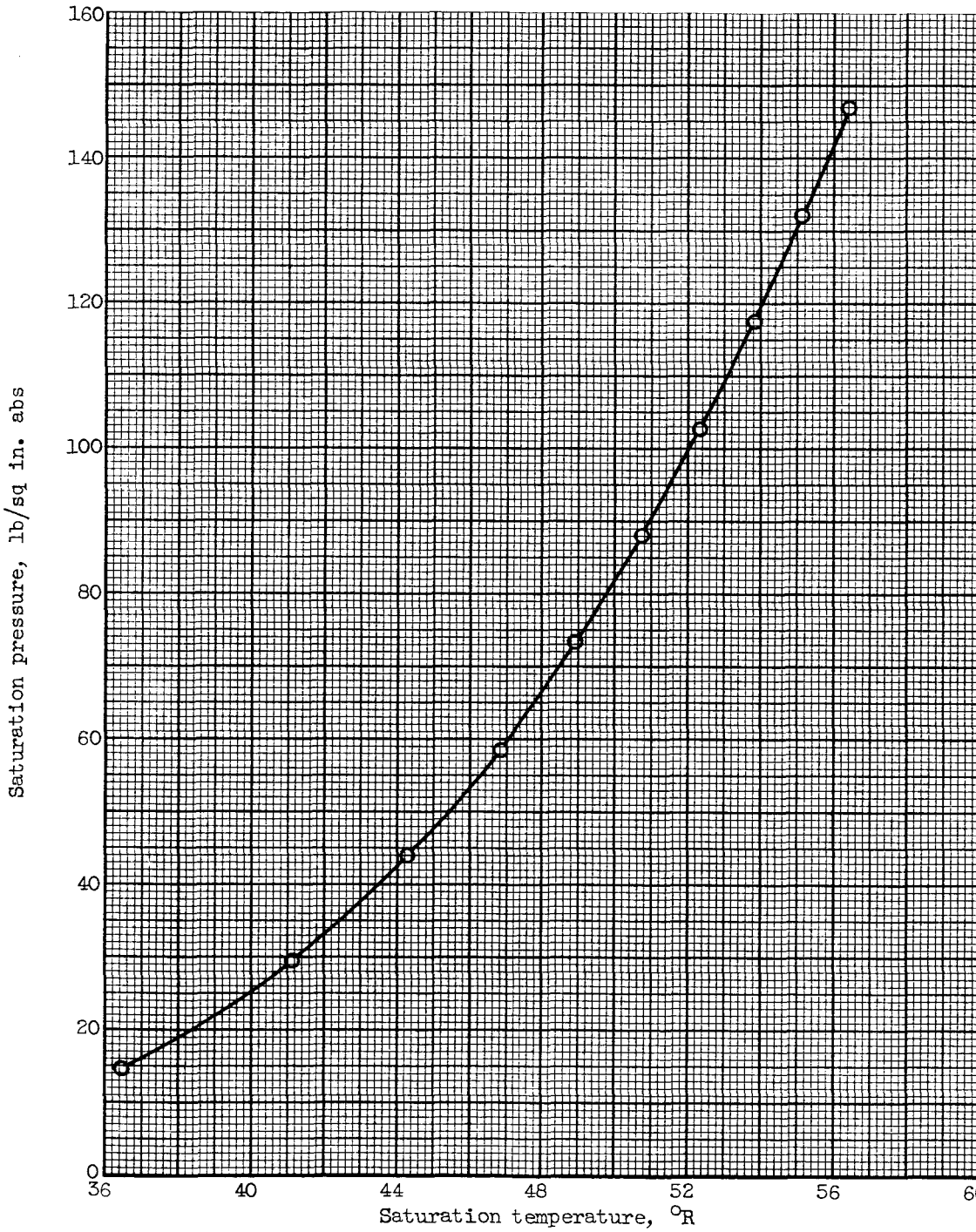

Figure 21. - Saturation temperature of para-hydrogen as function of pressure. Data from reference 20.

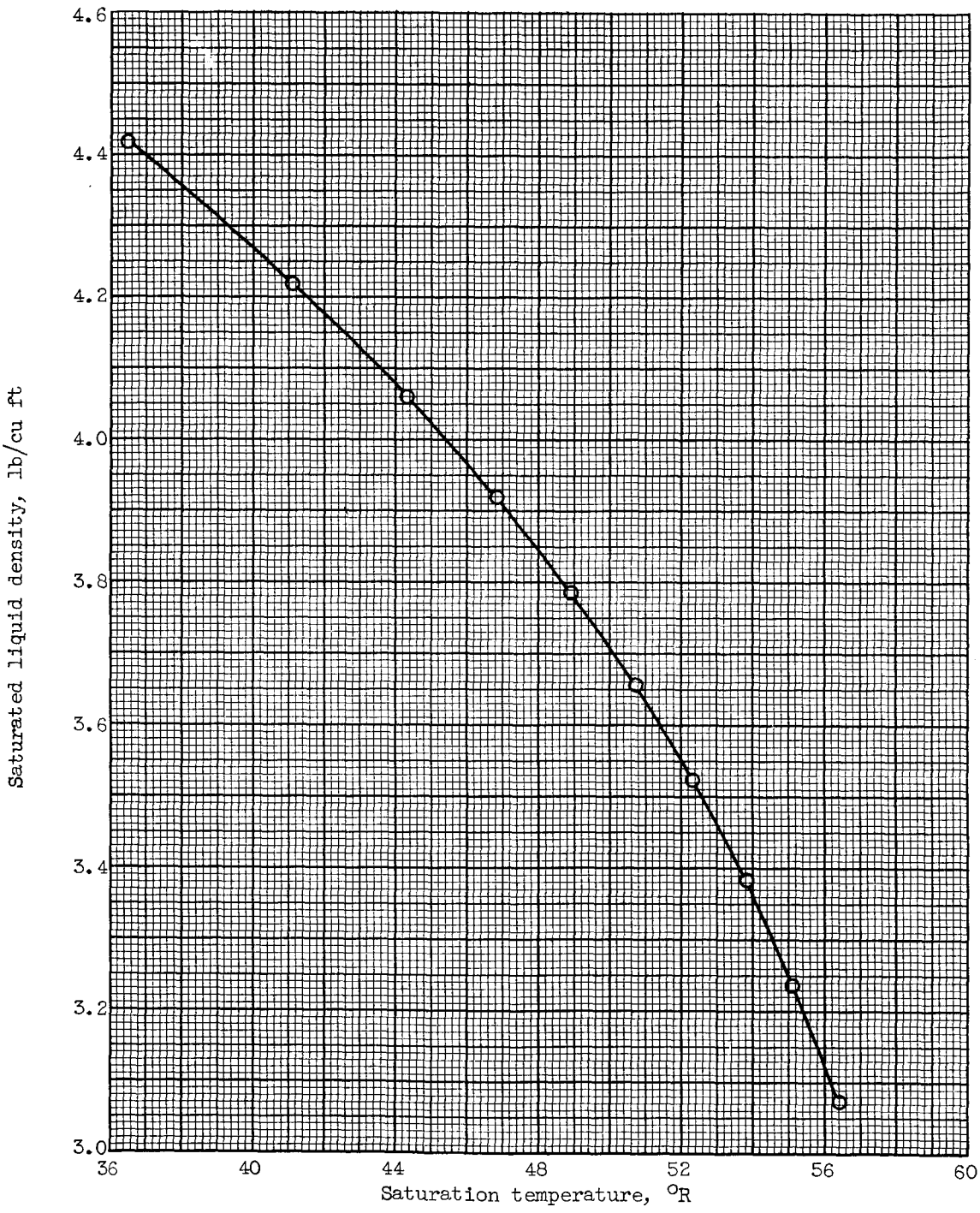

(a) Saturated liquid.

Figure 22. - Density of para-hydrogen as function of saturation temperature. Data from reference 20.

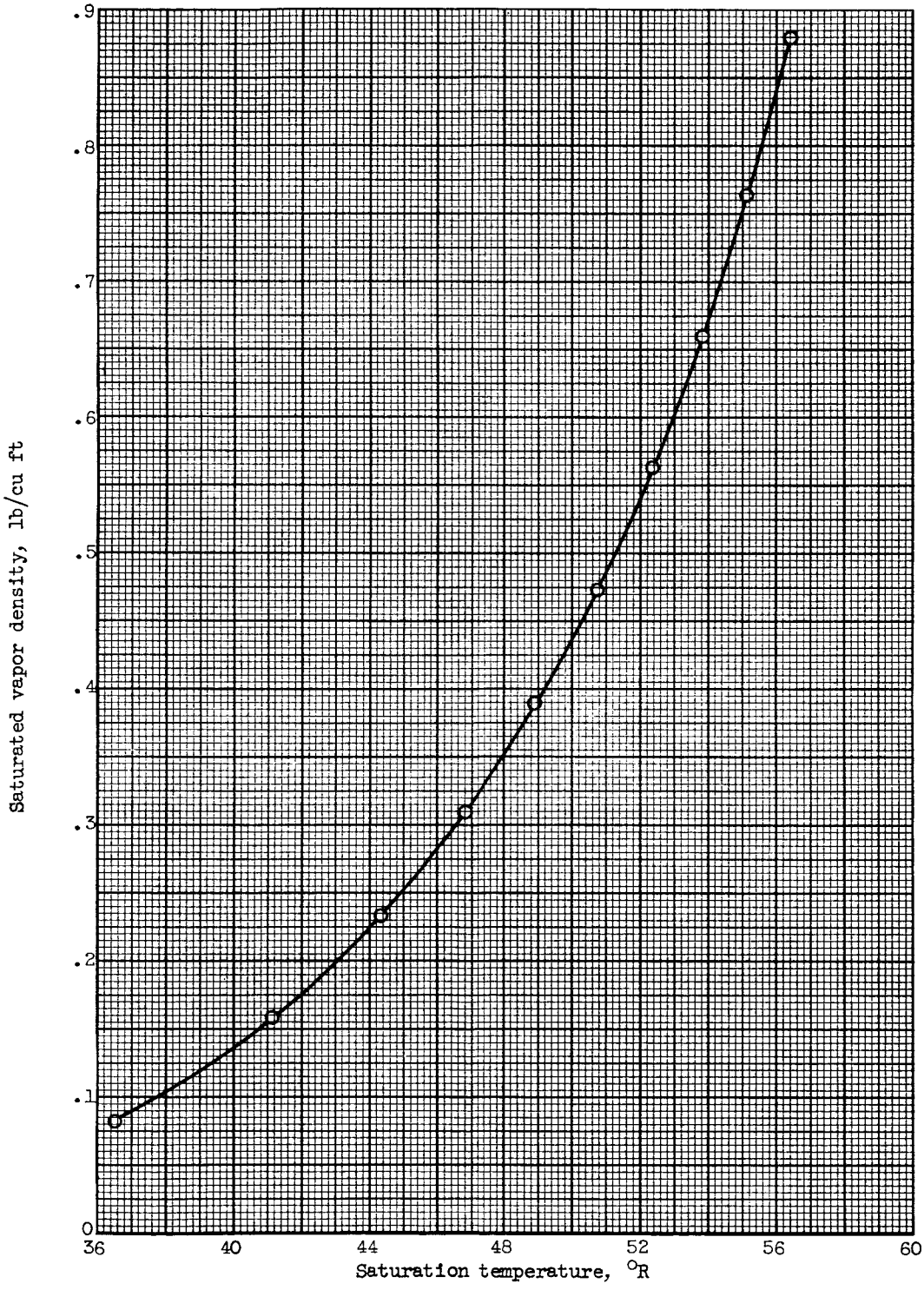

(b) Saturated vapor.

Figure 22. - Concluded. Density of para-hydrogen as function of saturation temperature. Data from reference 20.

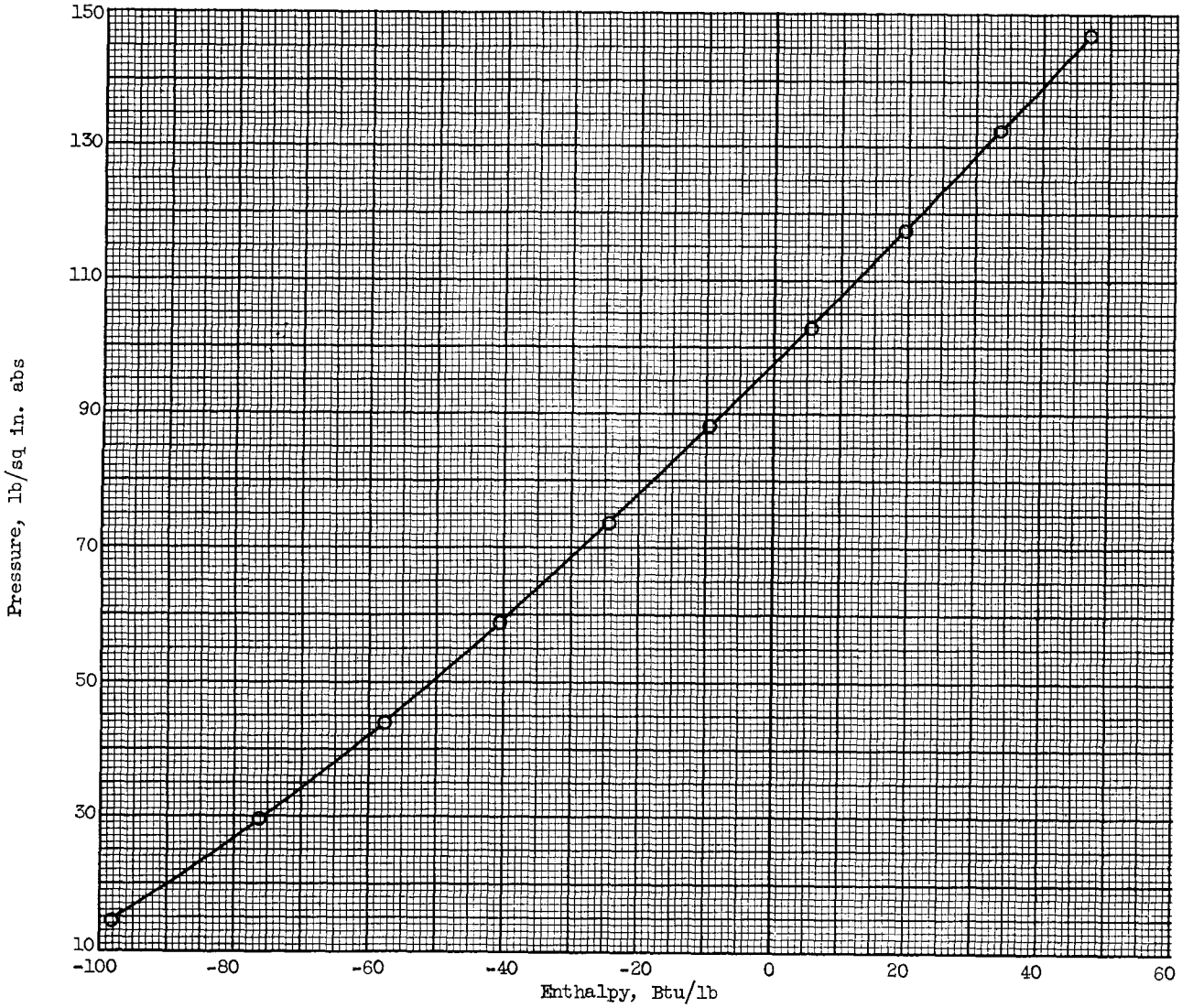

Figure 23. - Variation of enthalpy with pressure for specific volume of 0.9476 cubic foot per pound. Data from reference 20.

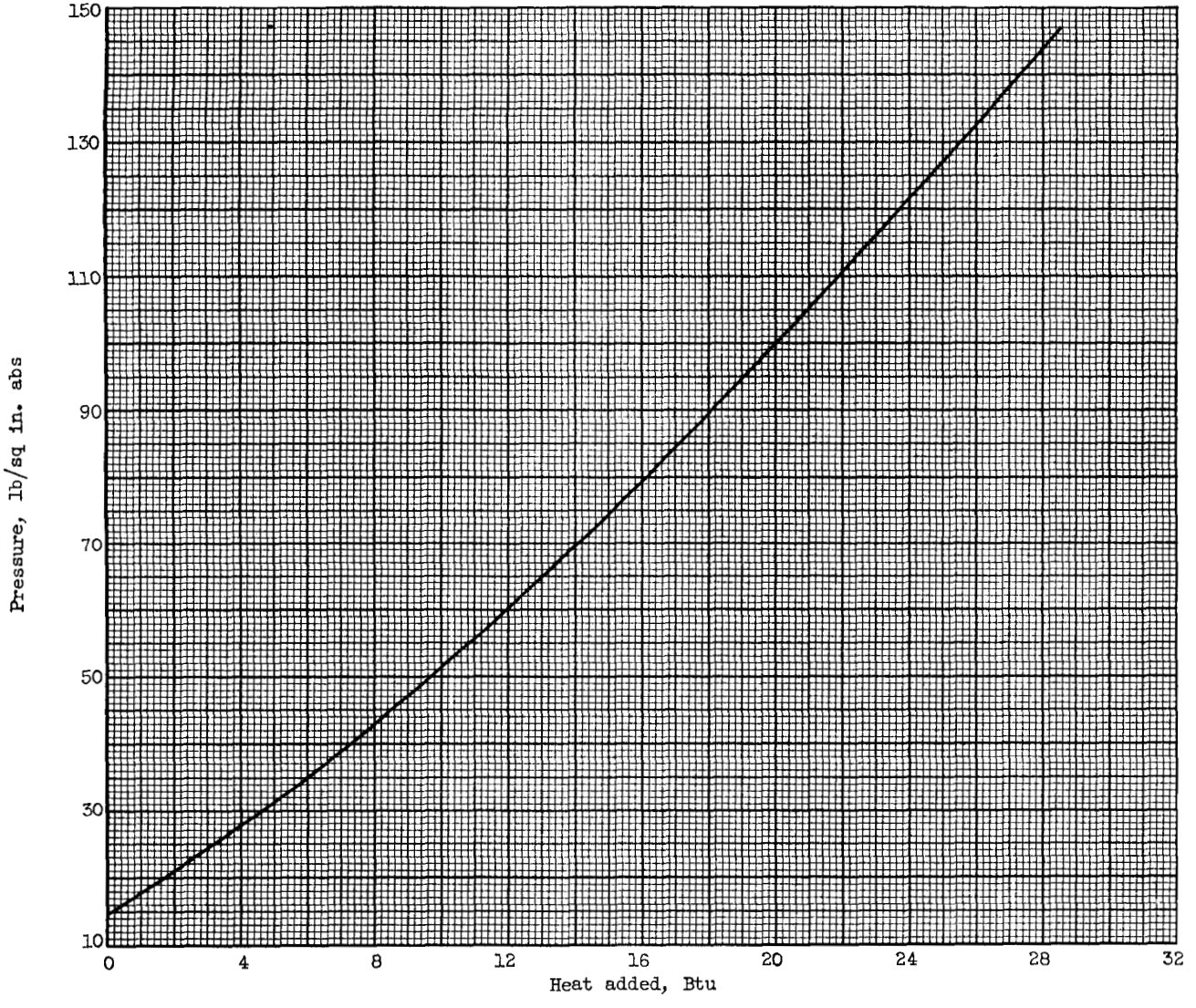

Figure 24. - Variation of pressure with heat added for specific volume of 0.9476 cubic foot per pound.

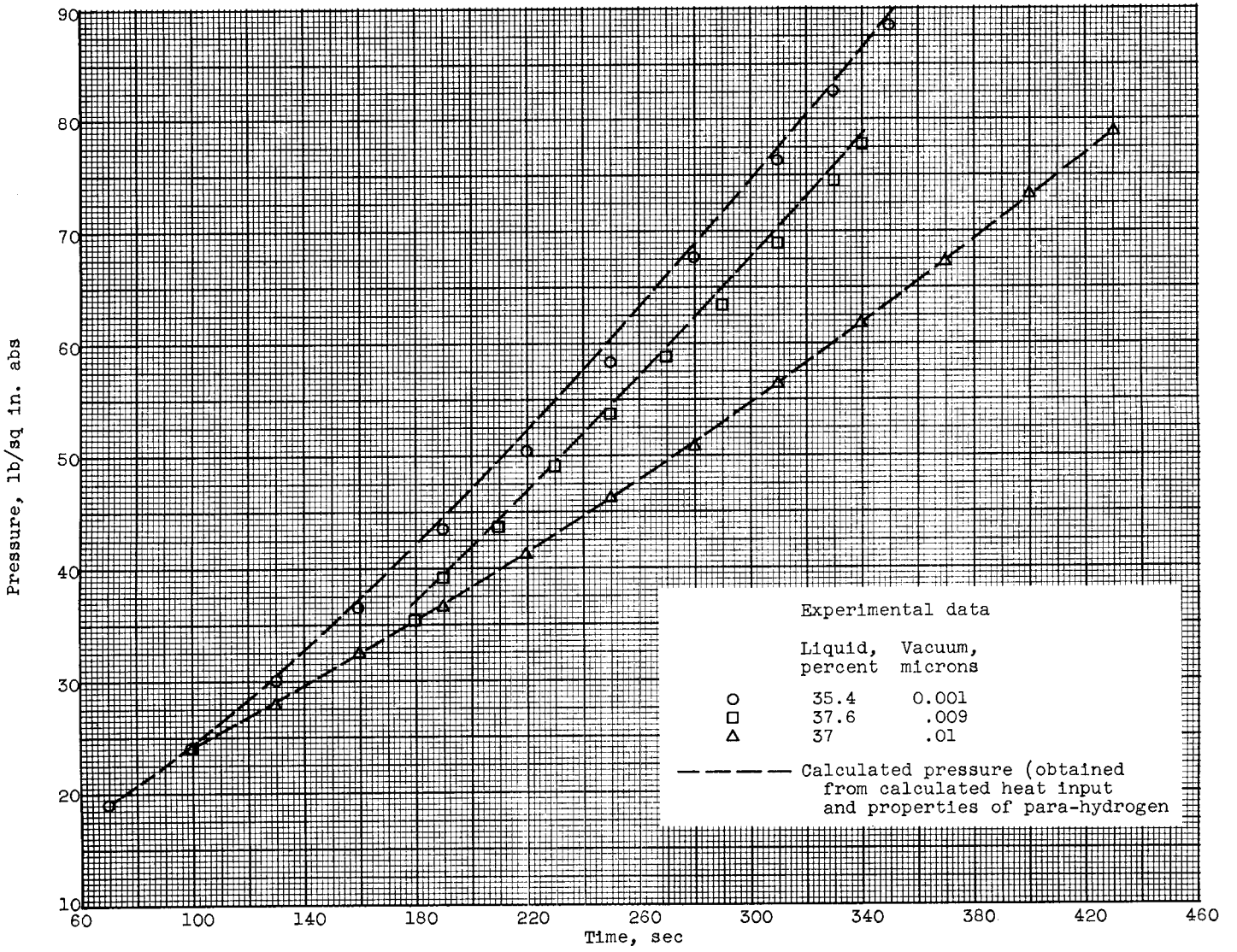

Figure 25. - Comparison of calculated pressure with experimental pressure.

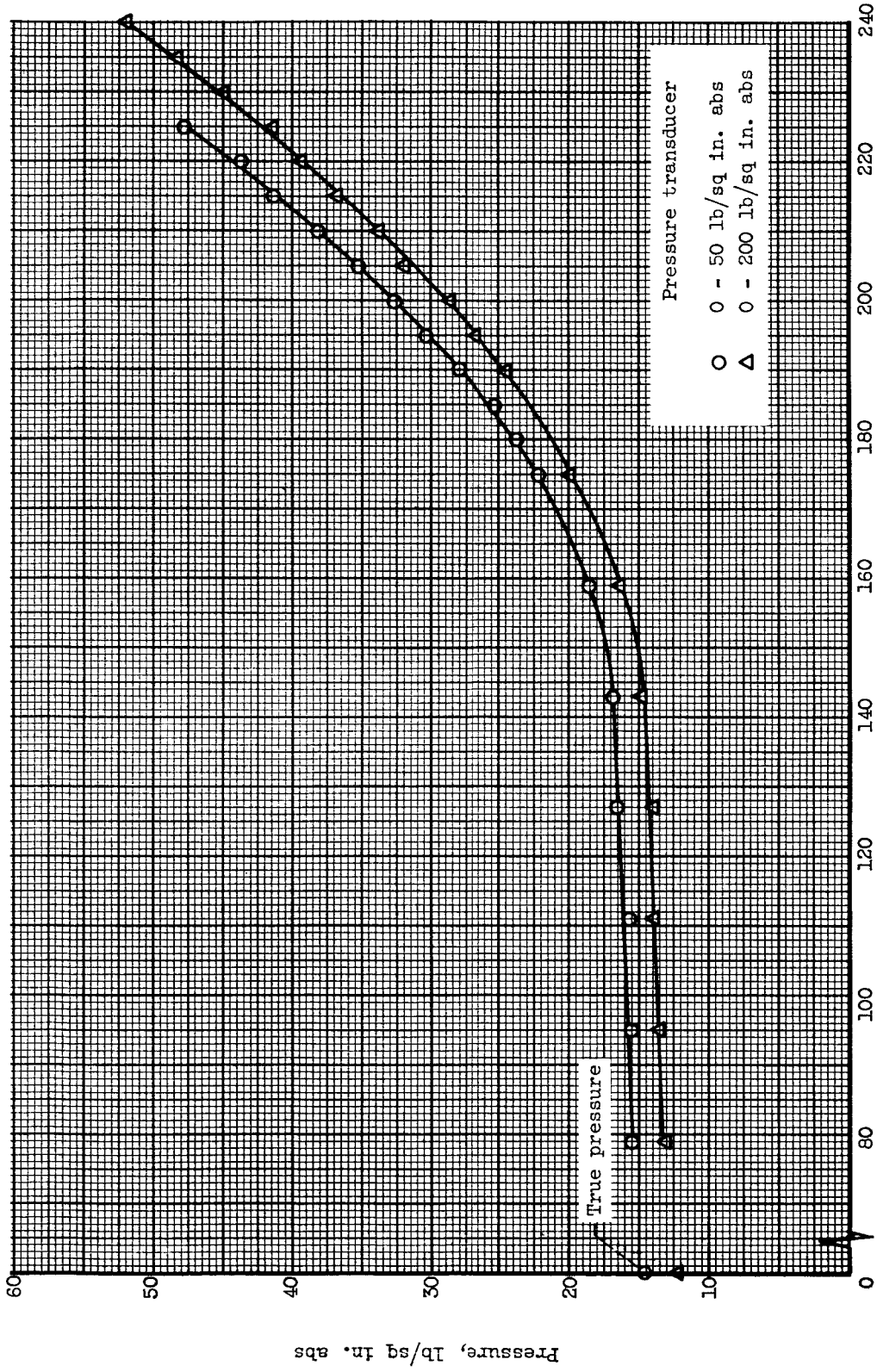

Figure 26. - Output of low- and high-pressure-range gages.